BMC Biology

RESEARCH ARTICLE Open Access

Dysregulation of innate immune signaling in animal models of spinal muscular atrophy

Eric L. Garcia[1,2], Rebecca E. Steiner[1,7,9], Amanda C. Raimer[1,10,3], Laura E. Herring[4], A. Gregory Matera[1,3,5,6,7*] and Ashlyn M. Spring[1,8*]

Abstract

Background Spinal muscular atrophy (SMA) is a devastating neuromuscular disease caused by hypomorphic loss of function in the survival motor neuron (SMN) protein. SMA presents across a broad spectrum of disease severity. Unfortunately, genetic models of intermediate SMA have been difficult to generate in vertebrates and are thus unable to address key aspects of disease etiology. To address these issues, we developed a *Drosophila* model system that recapitulates the full range of SMA severity, allowing studies of pre-onset biology as well as late-stage disease processes.

Results Here, we carried out transcriptomic and proteomic profiling of mild and intermediate *Drosophila* models of SMA to elucidate molecules and pathways that contribute to the disease. Using this approach, we elaborated a role for the SMN complex in the regulation of innate immune signaling. We find that mutation or tissue-specific depletion of SMN induces hyperactivation of the immune deficiency (IMD) and Toll pathways, leading to overexpression of antimicrobial peptides (AMPs) and ectopic formation of melanotic masses in the absence of an external challenge. Furthermore, the knockdown of downstream targets of these signaling pathways reduced melanotic mass formation caused by SMN loss. Importantly, we identify SMN as a negative regulator of a ubiquitylation complex that includes Traf6, Bendless, and Diap2 and plays a pivotal role in several signaling networks.

Conclusions In alignment with recent research on other neurodegenerative diseases, these findings suggest that hyperactivation of innate immunity contributes to SMA pathology. This work not only provides compelling evidence that hyperactive innate immune signaling is a primary effect of SMN depletion, but it also suggests that the SMN complex plays a regulatory role in this process in vivo. In summary, immune dysfunction in SMA is a consequence of reduced SMN levels and is driven by cellular and molecular mechanisms that are conserved between insects and mammals.

Keywords Neuromuscular disease; Traf6; Ubc13; NF-kB; Toll-like receptors, TLR; Tumor necrosis factor signaling, TNF; Innate immunity

*Correspondence:
A. Gregory Matera
matera@unc.edu
Ashlyn M. Spring
amspring2@uncg.edu
Full list of author information is available at the end of the article

Background

Spinal muscular atrophy (SMA) is a neuromuscular disease caused by mutations in the human *Survival Motor Neuron 1* (*SMN1*) gene and the accompanying reduction in levels of SMN protein [1]. In humans and SMA animal models, complete loss of SMN function does not lead to SMA; it causes developmental arrest and early lethality [2]. Hypomorphic point mutations in *SMN1* and/or reduced levels of full-length SMN protein cause the disease [3, 4]. The age-of-onset and severity of the disease varies widely, leading to a historical classification of SMA into three distinct subtypes, Type I (Werdnig-Hoffman disease, early infantile onset), Type II (intermediate late infant onset), and Type III (Kugelberg-Welander, childhood onset) [5, 6]. More recently, clinicians have increasingly recognized that SMA is better characterized as a broad-spectrum disorder, ranging from severe (prenatal onset) to nearly asymptomatic [7, 8]. SMA phenotypic severity is inversely proportional to SMN protein levels; however, the proximal trigger of the disease remains a mystery.

Mouse models of intermediate or late-onset SMA have been difficult to generate. Mutations at the endogenous mouse *Smn* locus or copy number changes in human *SMN2* (an *SMN1* paralog) transgenes cause dramatic shifts in phenotype from mild and largely unaffected [9–11], to very severe, with onset of symptoms in utero and death between 4 and 14 days [11–15]. To circumvent these problems, we developed a *Drosophila* model system [16, 17]. Using a series of SMA-causing missense alleles, we have shown that this system recapitulates the wide-spectrum of phenotypic severity seen in human patients [17–22]. Importantly, this system provides an opportunity to study all stages of the disease, from pre-onset biology to late-stage processes [20–22].

The phenotypes associated with *Drosophila* models of SMA include impaired locomotion, neuromuscular abnormalities, developmental delays, decreased viability, and reduced life span [16, 17, 20, 23–27]. In notable agreement with the onset of the human disease, our fruit fly models of SMA also exhibit progressive loss of limb motility, displaying a more rapid decline in posterior versus anterior appendages [20]. Additionally, specific mutations that affect the SMN Tudor domain were recently shown to affect SMN protein levels in a temperature-sensitive manner [21]. Hence, *Drosophila* models of SMA are continuing to reveal how individual mutations disrupt SMN function, contributing to different aspects of the disease.

The SMN complex chaperones the biogenesis of small nuclear ribonucleoproteins (snRNPs), core components of the spliceosome [28]. SMN carries out its functions in the assembly of snRNPs primarily in the cytoplasm [28]. *Smn* and *Phax (Phosphorylated Adaptor for RNA export)* null mutants exhibit an overlapping set of alternative splicing differences relative to wild-type animals [18]. Phax exports small nuclear RNAs (snRNAs) from the nucleus for assembly into snRNPs by the SMN complex [28, 29]. Recently, a common allele-specific *RpS21* alternative splicing event was shown to modify the larval lethality of *Phax*, but not *Smn*, mutants [30]. Transcriptomic profiling of various *Smn* null and missense mutants has revealed the activation of an innate immune response that correlates with phenotypic severity of the different mutants [18, 27]. Conspicuously, mutation of the *Phax* gene does not cause similar transcriptomic signatures of activated innate-immune signaling [18], which suggests that SMN may have a specific function in cellular immunity.

Defects in the development of immune cells and tissues have been reported in several mouse models of SMA [31–34]. These mice have smaller spleens and display altered red pulp macrophage morphology [32–34], events that reportedly precede evidence of neurodegeneration. More recently, dysregulation of innate immunity was reported in pediatric SMA patients, as they exhibit treatment-responsive changes in inflammatory cytokine profiles [35, 36]. Accumulating evidence suggests that SMN loss disrupts the immune system, contributing to excessive neuroinflammation and neurodegeneration.

Here, we show that the transcriptomes and proteomes of SMA model flies similarly display evidence of dysregulated innate immunity. Specifically, these SMA models exhibited an increase in transcripts and proteins involved in the *Drosophila* Immune Deficiency (IMD) and Toll signaling pathways. Concordantly, these animals also frequently displayed pigmented nodules (a.k.a. melanotic masses) that correlated with the molecular signatures of activated immune signaling. Knockdown of specific downstream targets of these signaling pathways ameliorated the formation of melanotic masses caused by *Smn* mutation or depletion. Overall, findings here suggest that SMN protein loss induces hyperactivation of innate immune signaling and a melanization defense response that correlates with the phenotypic severity of SMA-causing missense alleles.

Results

Quantitative proteomic analysis of Smn missense mutants identifies immune-induced peptides

Previously, we uncovered an increase in the expression of genes associated with innate immunity in the transcriptomes of *Smn* null and missense mutant fly lines [18, 27]; therefore, we sought to determine if the gene expression changes, identified by RNA-seq, are also reflected in the proteomes of hypomorphic *Smn* mutants. We therefore

carried out proteomic analyses using tandem mass tag labeling and mass spectrometry (TMT-MS) on protein lysates from whole wandering third instar larvae. Animals expressing either Flag-*Smn* wild-type (WT) or SMA-causing missense mutant transgenes as their sole source of SMN protein were used. The transgenes were each inserted at the same ectopic locus and driven by the native *Smn* promoter in an otherwise $Smn^{X7/X7}$ null background [16, 17]. We employed two different SMA patient-derived mutations located in distinct subdomains of the SMN protein, the Tudor domain ($Smn^{Tg:V72G}$) and the tyrosine- and glycine-rich YG Box ($Smn^{Tg:T205I}$); see Fig. 1A. The Tudor domain of SMN binds symmetric dimethylarginine residues present at the C-termini of Sm proteins [37, 38], and the YG Box functions in SMN self-oligomerization [19, 22, 39, 40]. As previously described

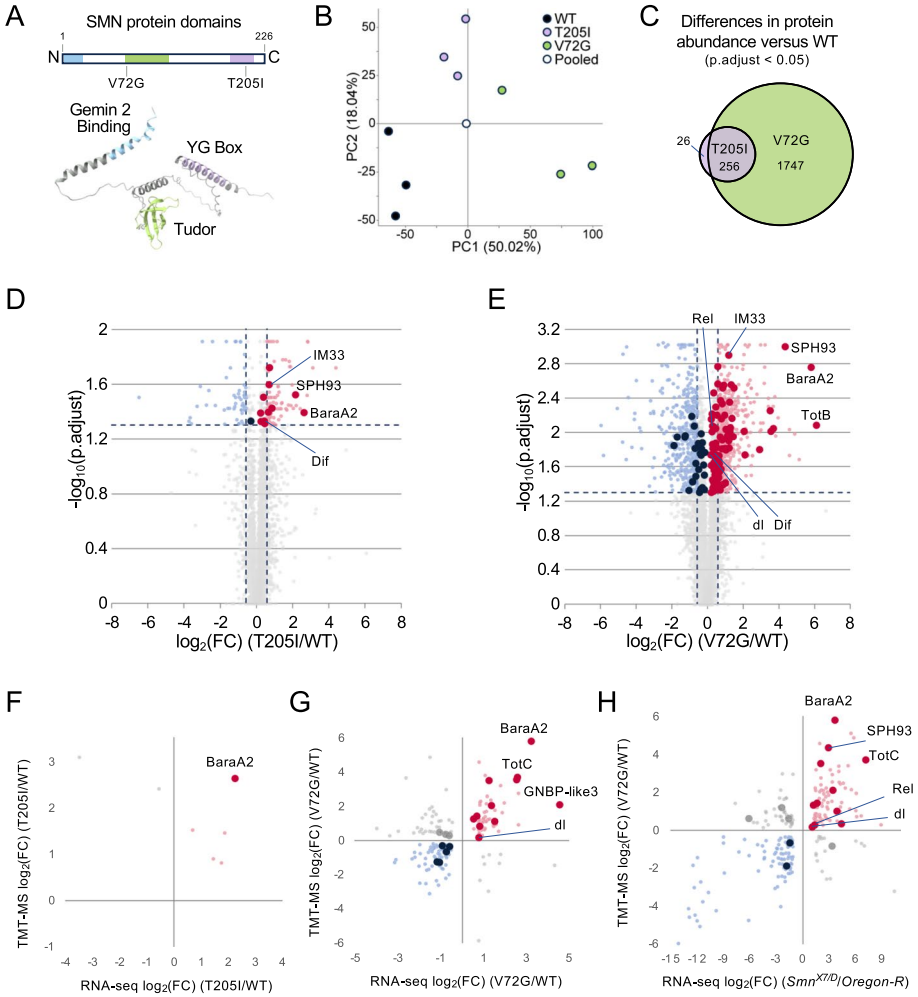

Fig. 1 The proteomes and transcriptomes of *Drosophila Smn* hypomorphs provide overlapping evidence for innate immune activation. **A** A rectangular cartoon and an AlphaFold model of the relative positions of conserved domains of the *Drosophila* SMN protein and the location of the patient-derived missense mutations used here. **B** Principal component analysis of total protein abundances in the *Smn* transgenic lines. *Smn* lines: WT ($Smn^{X7/X7}$,Flag-$Smn^{Tg:WT}$); T205I ($Smn^{X7/X7}$,Flag-$Smn^{Tg:T205I}$), Tyrosine (T) to Isoleucine (I); and V72G ($Smn^{X7/X7}$,Flag-$Smn^{Tg:T205I}$), Valine (V) to Glycine (G). **C** Venn diagram of overlapping protein differences in T205I and V72G relative to WT. **D** Volcano plot of protein differences in the T205I line relative to WT. Proteins associated with innate immunity are indicated by larger dots. **E** Volcano plot of protein differences in the V72G line relative to WT, and proteins associated with innate immunity are labeled as in **D**. Dashed vertical bars in **D** and **E** indicate a Log2 FC ratio of ± 0.58, and the horizontal dashed line corresponds to *q*-value = 0.05. **F** Comparison of T205I proteome (*y*-axis) with T205I transcriptome (*x*-axis). The proteome and transcriptome are relative to the WT genotype. **G** Comparison of V72G proteome (*y*-axis) with V72G transcriptome (*x*-axis). As in **F**, the proteome and transcriptome are relative to WT. **H** V72G proteome (*y*-axis) versus $Smn^{X7/D}$ null transcriptome (*x*-axis). The differential gene expression of the $Smn^{X7/D}$ transcriptome is relative to *Oregon-R*. Note that the total (Ribo-minus) RNA-seq data [18] on the *Smn* hypomorphs were originally generated with the intent to measure non-coding RNA levels (specifically, spliceosomal snRNAs) and are therefore not as deep as one might like to use for measuring mRNAs, particularly the lowly-expressed ones. The *Smn* null datasets were polyA-selected and are thus better able to detect changes in mRNA levels

[20, 21], T205I is a Class 3 mutation (semi-lethal, ~ 10% eclosion), whereas V72G is more severe and is categorized as a Class 2 mutation (inviable at 25 °C, all die as early pupae).

Overall, 5857 *Drosophila* proteins were identified using TMT-MS (Tables S1–S3). Principal component analysis of TMT-MS quantified protein abundances showed good covariance levels (an average of ~ 10% per sample) for the three different *Smn* transgenic lines we tested: WT, V72G, and T205I (see Fig. 1B for detailed genotypes). Among the proteins quantified, only 282 proteins were differentially expressed (p.adj < 0.05, $\log_2$ fold change ± 0.5) in the T205I mutant relative to WT control (Fig. 1C, D). Note that the control animals expressing the WT rescue transgene are known to be slightly hypomorphic to begin with [17, 20], so that may account for the small number of observed differences. In contrast, the V72G mutant exhibited 2003 differentially expressed proteins relative to WT control (Fig. 1C, E). Most of the protein abundance differences found in the T205I mutant (90%) were also seen in the V72G mutant (Fig. 1C). The V72G and T205I hypomorphs each display significant defects (in viability, locomotion, etc.) relative to the WT controls, but the phenotype of the V72G animals is more severe than that of T205I [17, 20]. Thus, the observed changes in protein abundance correlate with overall phenotypic severity (Fig. 1D, E).

Immune dysregulation lies at the intersection of SMA model proteomes and transcriptomes

We took advantage of an early pupal RNA-seq dataset [18] we had previously generated for *Smn* WT, T205I, and V72G animals (Tables S4-S5) to carry out a multi-omic analysis of transcriptomes and proteomes. Although the TMT-MS experiment detected only a subset of the genes that can be analyzed by RNA-seq (e.g., 6000 vs. 13,000), proteins that were significantly altered in the mutants also tended to display a similar trend on the transcriptome level. To this end, correlation plots of the log2 fold change ratios of the TMT-MS vs. total RNA-seq datasets showed good overall agreement between differences in RNA and protein abundance relative to the WT control (Fig. 1F, G).

Even though the milder T205I (Class 3) mutant had only ~ 300 detectable changes at the protein level, and only seven overlapping RNA and protein changes (Fig. 1F), most of these (five out of seven) were increased in the T205I compared to WT. Notably, this includes the *Baramicin* locus (containing two identical genes, *BaraA1* and *BaraA2*) that encode an immune-induced antifungal peptide [41, 42]. For simplicity, we refer to all transcripts and proteins that mapped to this locus as *BaraA2 or* BaraA2, respectively (Fig. 1F). By comparison, the overlapping differences between the transcriptome and proteome of the more severe V72G (Class 2) mutant include increases in numerous immune-induced and stress-responsive gene products (Fig. 1G). We note that analysis of the T205I transcriptome identified increases in many of these same immune-induced molecules that were not captured by TMT-MS (Table S4). Strikingly, we observed small but significant increases in core upstream signaling factors like the NF-kB ortholog dorsal (dl) and larger increases in defense-responsive and downstream stress-responsive targets like BaraA2, Turandot C (TotC), and Gram-negative bacteria binding-like protein 3 (GNBP-like3). Hence, our multi-omic approach further highlights the hyperactivation of innate-immune signaling that accompanies partial SMN loss-of-function.

For additional comparisons to the *Smn* missense mutant proteomes, we used polyA + -RNA-seq datasets from two different *Smn* null mutant lines [27, 43]; see Tables S6–S11. The $Smn^{X7/D}$ null mutant transcriptome identified an increase in *BaraA2* and *SPH93* (*Serine protease homolog 93*) transcripts in both T205I and V72G proteomes (Fig. 1H and Tables S1–S3). The overlap between the $Smn^{X7/D}$ transcriptome and the V72G proteome was even more remarkable and included the core NF-kB-like factor, Rel (Fig. 1H and Table S11). Thus, the overlapping differences between the *Smn* null and missense mutants suggest that the observed hyperactivation of immune signaling is a common feature of SMN loss.

A key strength of this multi-omic approach is the ability to detect mRNA and protein isoform-specific differences. For this analysis, we employed an additional, probabilistic RNA-seq pipeline to quantify discrete mRNA isoforms and maintain pseudoalignment information from different splice junctions, but with a focus on differential expression of transcripts [44, 45]. Quantification of discernable transcript differences between *Smn* null and control animals revealed an increase in numerous transcripts associated with innate immunity in the mutants (Fig. S1A-B). Differences included changes in transcripts and proteins involved in innate immunity, such as the NF-kB orthologs dorsal (dl), Dorsal-related immunity factor (Dif), and Relish (Rel); see Fig. S1A-B.

Most striking, a comparison of the V72G proteome with the *Smn* null transcriptome revealed parallel isoform-specific changes for numerous transcripts and proteins (Fig. S1C). The congruent changes in RNA and protein isoforms included changes in molecules involved in innate immunity, including SPH93-RA/PA, TotC-RA/PA, GNBP-like3-RA/PA, and Dif-RC/PC (Fig. S1C). In summary, the identification of overlapping changes in specific transcripts and protein isoforms further supports the activation of immune signaling in fly models of SMA.

Partial loss of SMN function causes hyper-activation of innate immunity

SMA is a hypomorphic condition; total loss of function causes early developmental arrest and lethality [12], reviewed in [2]. As detailed widely in the literature, *Smn* null mutants are therefore poor disease models. Hence, we focused our efforts to identify drivers of the observed innate immune dysfunction on the *Smn* hypomorphs. Gene ontology (GO) analysis of protein abundance differences in the V72G dataset revealed a broad dysregulation of factors involved in pathogen defense response and innate immune signaling pathways (Fig. 2A and Tables S12–S13). These include proteins involved in melanization and humoral defense responses to bacterial, fungal, and viral pathogens (Fig. 2A, B). Although the V72G mutant exhibited numerous increases in

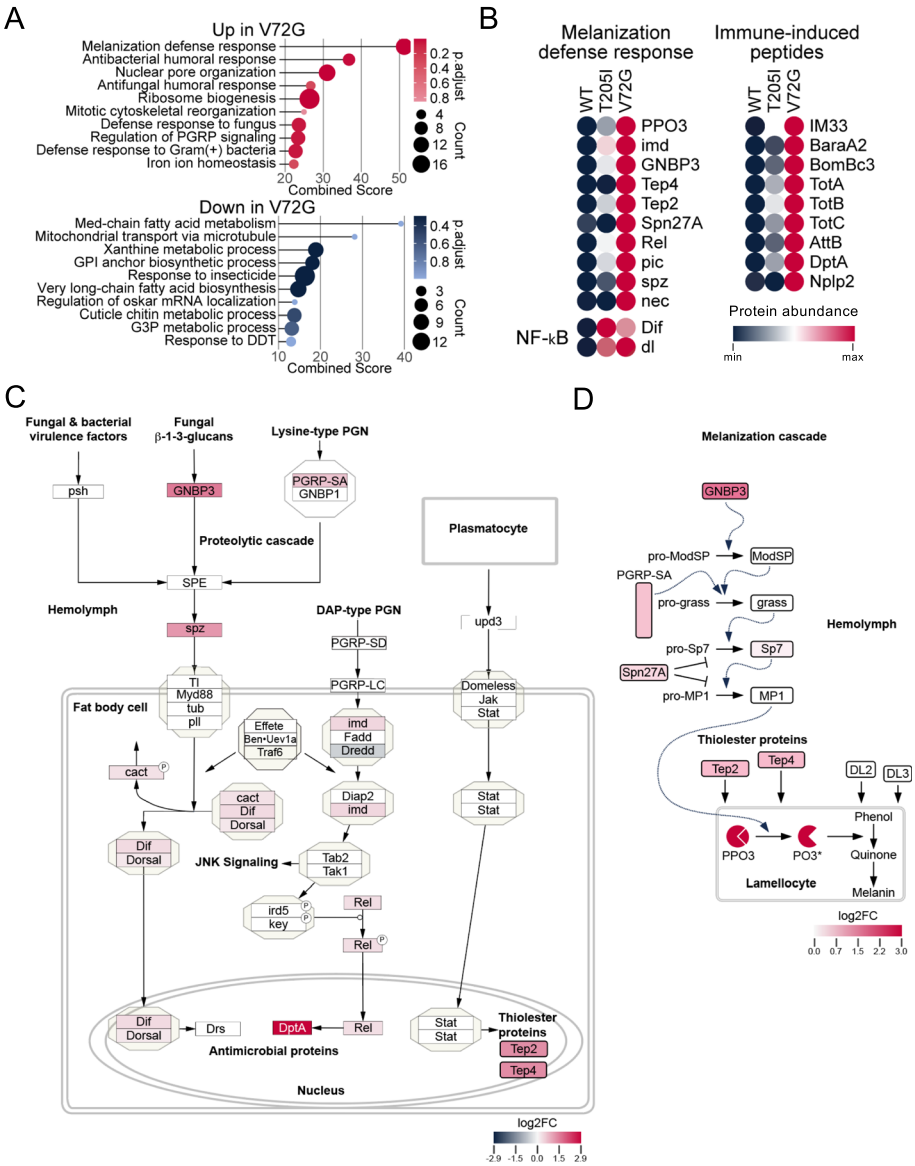

Fig. 2 Proteins involved in *Drosophila* humoral and melanization defense responses are elevated in *Smn* mutant proteomes. **A** Gene Ontology (GO) analysis of protein differences in V72G. Adjusted *p*-values (p.adjust) and number of genes per GO term (Count) are shown at right, which is used to compute a combined score. **B** Heat maps of select protein abundance differences from genes within the melanization defense response GO category, known immune-induced peptides, as well as for the NF-kB transcription factors dorsal-related immunity factor (Dif) and dorsal (dl). **C**, **D** Heatmap illustrations of TMT-MS data from V72G mutants. Log_2-fold change (log2FC) values (mutant/control) for differentially expressed proteins are illustrated within the context of the Humoral Immune Response pathway (panel **C**, Wikipathways, WP3660) or the Melanization Cascade pathway (panel **D**) and shaded according to their respective keys

proteins involved in defense response pathways, a few of these proteins were also significantly upregulated in the less severe T205I animals (Fig. 2B). Importantly, both mutants displayed small but significant increases in NF-κB transcription factor levels (Fig. 2B).

Upregulation of defense response proteins occurs in the absence of an external immune challenge, supporting the notion that partial loss of SMN function causes hyper-activation of innate immune signaling. Consistent with this hypothesis, we frequently observed black, melanotic spots or granules in third instar *Smn* missense mutant larvae. Such granules are commonly referred to as pseudotumors, melanotic tumors, or melanotic masses [46, 47]. These structures typically form in response to pathogens, tissue damage, and necrosis, but this defense response can also be triggered by different genetic perturbations [46, 48–50].

Irrespective of the trigger, melanotic masses often form in the larval hemolymph and can be readily observed through the transparent body wall [46]. We therefore carried out a systematic analysis of larval melanization (Fig. 3) in a battery of ten hypomorphic, SMA-causing *Smn* missense alleles developed in our laboratory [17, 20]. To quantify this phenotype, we scored both the size and number of melanotic masses in 50 wandering third instar larvae for each genotype. All lines examined displayed a statistically significant and robust increase in the presence of melanotic masses relative to the Oregon-R (OreR) controls (Fig. 3A). Larvae with a WT Flag-*Smn* transgene exhibited significantly fewer melanotic masses than *Smn* missense mutant lines but more than OreR (Fig. 3A), consistent with our previous observations that the *Smn* WT transgenic line is mildly hypomorphic [17, 20]. Size scoring (Fig. 3B, C) and counts of the total number of melanotic masses per animal (Fig. 3D) show similar trends to the overall incidence of masses. Furthermore, the number of melanotic masses for the various SMA-causing missense lines correlated with the previously characterized phenotypic severity (Fig. 3E) [20]. These observations suggest that the function of SMN in immune tissues is conserved from flies to mammals and that *Smn* mutations in the fly can be used to model peripheral defects of SMA in addition to the canonical neuromuscular phenotypes.

The SMN-dependent hyper-activation of melanization is tissue-specific

To determine if the melanotic masses in fly models of SMA are downstream effects of tissue-specific SMN loss, we used the *Drosophila* GAL4/UAS system and RNA interference (RNAi) to deplete SMN in specific tissues [51]. We and others have previously employed this system to create partial SMN loss-of-function models that typically cause pupal lethality, although weakly viable adults can be obtained if the RNAi is performed at a lower temperature, e.g., 25 °C (see [20, 52]). Here, we employed two different *UAS:Smn* short hairpin (sh)RNA lines, P|TRiP.JF02057|attP2 (Smn^{JF}-RNAi) and P|TRiP.HMC03832|attP40 (Smn^{HM}-RNAi), at 29 °C. Using a *daughterless* GAL4 driver (*da-Gal4*), we found that systemic SMN knockdown recapitulated the effects of the *Smn* missense mutations described above (Fig. 4A). Melanotic mass formation was dependent upon shRNA expression, as negative control lines (Gal4 driver-only, UAS:responder-only or OreR) showed no significant effects (Fig. 4A).

In *Drosophila*, the immune response is coordinated by the fat body, an organ that is functionally analogous to the mammalian liver and adipose tissue [55, 56]. The fat body signals to a group of macrophage-like cells, collectively called hemocytes [50]. The molecular pathways and mechanisms that regulate hemocyte/macrophage development and activity are conserved from flies to humans [48–50]. When activated, hemocytes encapsulate invading particles and melanize them to sequester and kill pathogens [50]. Depletion of SMN within the fat body and hemocytes (using *Cg-Gal4*) led to both a high frequency and number of melanotic masses per animal (Fig. 4A–C). In contrast, the knockdown of SMN throughout the larval neuromusculature (using *C15-Gal4*) had no significant effect (Fig. 4A, C). Thus, the appearance of melanotic masses following depletion of SMN within immune cells rather than in neurons or muscles suggests that this phenotype is not a downstream consequence of neuromuscular dysfunction.

To ascertain whether melanotic mass formation was a consequence of SMN depletion within hemocytes, we carried out additional assays using the *Hemolectin-Gal4 (Hml-Gal4)* driver. As shown in Fig. 4D and E, knockdown of SMN specifically within hemocyte lineages also resulted in the formation of larval melanotic masses. Therefore, we conclude that the observed melanization phenotype in response to SMN loss is derived from cell-type specific defects in immune cells.

Signaling pathways that regulate SMN-dependent melanization

To measure the relative contribution of various genes and pathways to the formation of melanotic masses induced by SMN knockdown, we next carried out a series of genetic modifier assays. Given the results in Fig. 4, and the well-known function of the fat body in synthesizing and secreting antimicrobial peptides (AMPs) into the hemolymph [57], we focused our screening efforts using the *Cg-Gal4* driver to reduce SMN levels by RNAi and

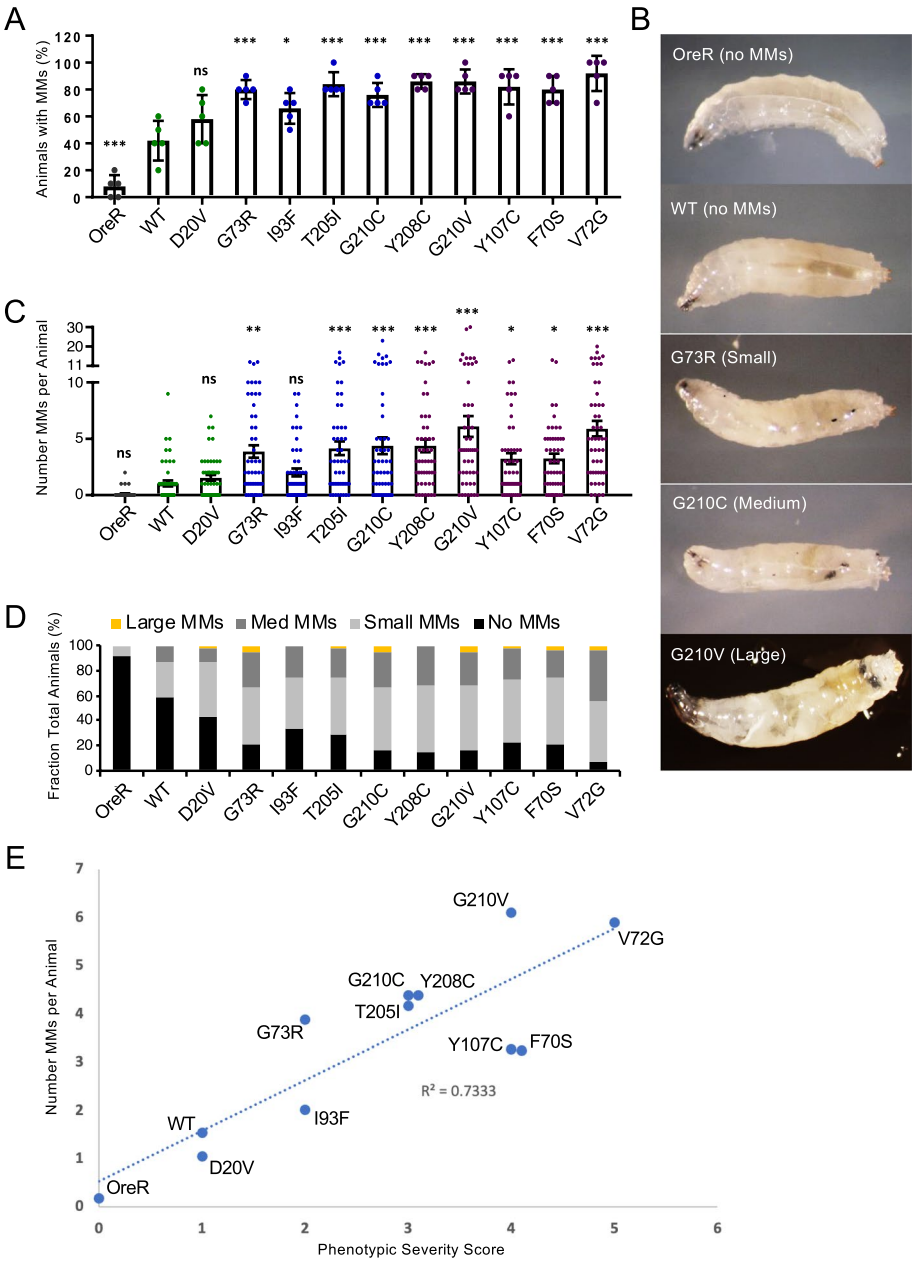

Fig. 3 *Smn* missense mutants exhibit elevated melanotic masses. **A**–**C** Melanotic mass (MM) data for wandering third instar larvae expressing *Smn* missense mutations. The data in each panel are a different measure of the melanotic mass phenotypes of the same set of larvae. **A** Percent of larvae with one or more melanotic mass. Individual data points are the percent of larvae with MMs, 10 larvae per data point. **B** The average number of melanotic masses per animal. Data points show the number of MMs in each animal. Number (*N*) = 50 larvae for each genotype. **C** Qualitative size scoring of the largest melanotic mass in each larva. **D** Representative images of MMs in animals expressing *Smn* missense mutations. Bars show the mean, and error bars show the standard error of the mean. Asterisks indicate *p*-values relative to WT: * < 0.05; ** < 0.01; and *** < 0.001. **E** Graph showing correlation between the overall phenotypic severity of SMA-causing *Smn* missense mutations and the number of MMs per animal (from panel **B**). SMA-like phenotypic severity scores were assigned for each allele (zero being the mildest) based on previously published viability and locomotor assays [20]. Dotted line shows linear regression between data points along with a goodness-of-fit coefficient (R^2)

then crossed in various mutations or secondary shRNA transgenes into this background.

The Toll, IMD, and TNF (Tumor Necrosis Factor-alpha, called Eiger in flies) signaling pathways (Fig. 5A) use NF-kB transcription factors (dl, Dif, and Rel) to turn on AMP genes [55, 57–59]. Based on our multi-omic evidence (Figs. 1 and 2) showing overexpression of these NF-kB orthologs in our SMA models, we first ingressed

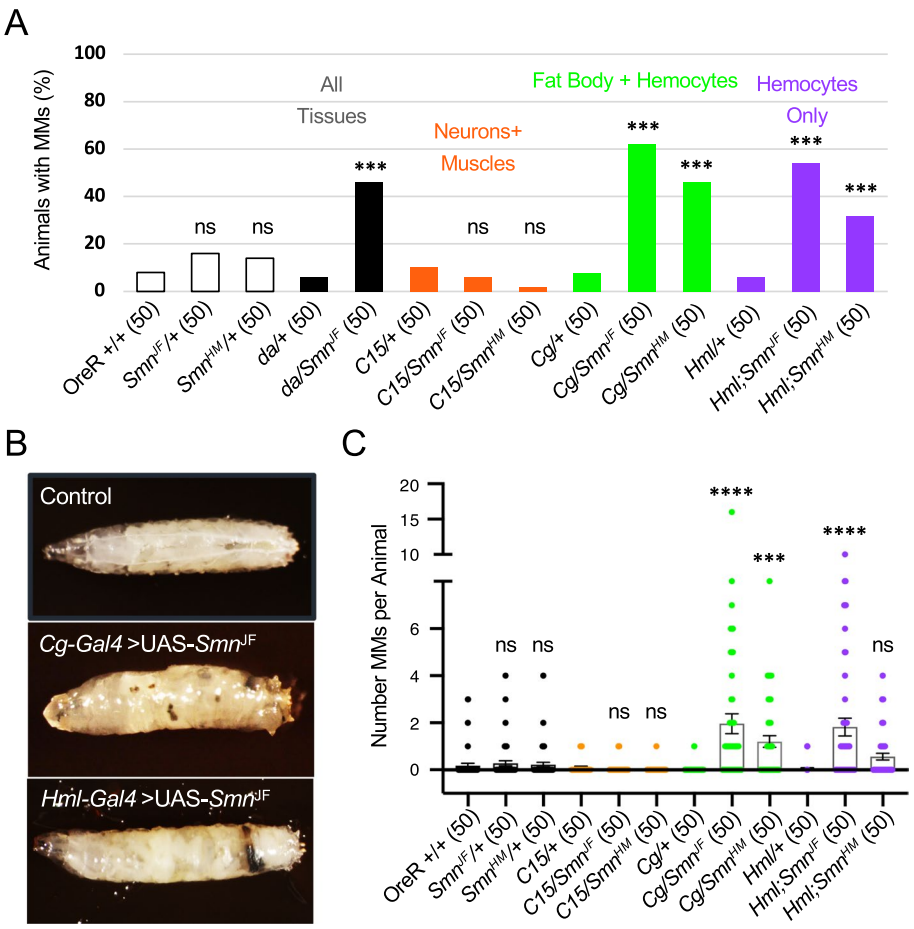

Fig. 4 Targeted RNAi depletion of *Smn* in *Drosophila* immune cells yields melanotic masses and reduced viability. **A** Fraction of larvae that display MMs. RNAi-mediated knockdown of SMN was carried out using the *Drosophila* GAL4/UAS system to drive expression using two different RNAi transgenes, UAS-Smn^{JF} (P|TRiP.JF02057|attP2) or UAS-Smn^{HM} (P|TRiP.HMC03832|attP40). These lines were used together with the following GAL4- drivers: *da*, *daughterless* (*da*) for ubiquitous knockdown; *C15* (a composite driver that includes *elav-* (*embryonic lethal abnormal vision*), *sca-* (*scabrous*) and BG57-GAL4 for knockdown in both neurons and muscles [53]; and *Cg* (*Collagen 4a1 gap*), for knockdown in the fat body, hemocytes, and the larval lymph gland [54]. OreR is the control strain. A plus sign (+) indicates a wild-type chromosome. **B** Representative image of wild-type control and MMs in a larva with SMN depleted in the fat body, hemocytes, and lymph gland (*Cg-Gal4 > UAS-*Smn^{JF}) or only in the hemocytes (Hml-Gal4 > *UAS-*Smn^{JF}). **C** Number of MMs per animal with and without SMN depletion, as in **A**

heterozygous mutations for *dl* and *Rel* into the background of *Cg-Gal4/*Smn^{IF}-RNAi flies to reduce dosage of these genes and then scored the resultant progeny for melanotic masses. As shown in Fig. 5B, mutants for *dl* and *Rel* suppressed the phenotype, reducing the average number of melanotic masses per larva. We also tested the dl/Dif regulatory factor, cactus. Contrary to our expectation, the reduced dosage of cactus also reduced the number of melanotic masses. Mutations in *cactus* alone can cause melanotic masses [46]. However, because cactus levels are elevated in T205I and V72G animals (log2FC = 0.26) and the well-documented autoregulatory feedback loop for this protein [60], the mechanism of action is unclear. Nevertheless, these data show that reducing gene dosage of downstream targets can suppress the melanization phenotype but throughput for this assay is quite low, often requiring generation of recombinants, and is limited by the genomic locations and availability of mutations of target genes.

To expand the scope of the investigation, we employed an RNAi-based candidate approach that couples *Cg-Gal4* mediated knockdown of *Smn* with the co-depletion of other factors. As a negative control for potential titration of GAL4 (which could reduce the efficacy of *Smn* knockdown), we co-expressed a UAS:NLS-GFP transgene. As shown in Fig. 5C, co-expression of a second UAS responder construct had no effect on the number of melanotic masses in the control larvae. In contrast,

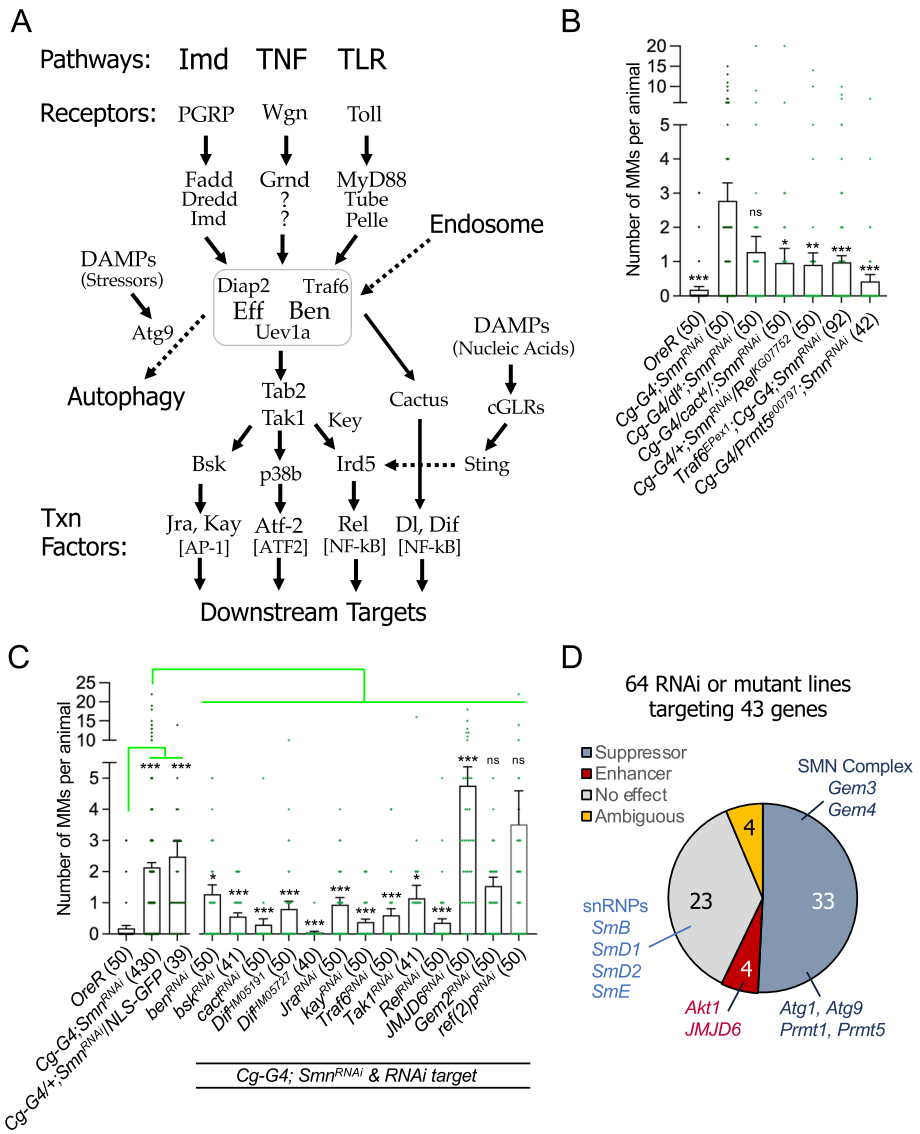

Fig. 5 Innate immune signaling pathways contribute to MMs upon SMN depletion. **A** Diagram summarizing the features and interconnections between innate immune signaling pathways in *Drosophila*. Bendless/Ubc13 (Ben) is an E2 ubiquitin conjugase that heterodimerizes with Uev1a and functions in a complex (boxed in gray) with Effete/Ubc5 (another E2) and two different E3 ligases (Traf6 for TLR/Toll or TNF/Wgn, and Diap2 for the Imd/PGRP pathway). The Immune Deficiency protein (Imd) serves not only as a receptor-proximal signaling factor, but also as a secondary substrate for K63-linked polyubiquitylation via Ben•Uev1a. Bendless thus sits at a node that connects many different signaling pathways and cellular processes. **B** Mutations in the IMD and Toll signaling pathways suppress the number of MMs per animal in *Smn* RNAi lines. Reduced dosage of *Protein Arginine Methyltransferase 5* (*PRMT5*) also suppresses MMs upon depletion of SMN. **C** MMs per animal were measured following co-expression of an *Smn* RNAi transgene together with the indicated RNAi lines targeting selected members of the Toll and IMD pathways, as well as to genes encoding the *Jumonji domain containing 6* (*JMJD6*), *Gemin 2* (*Gem2*), and *refractory to sigma P* (*ref(2)P*) proteins. Co-expression of UAS:NLS-GFP was used as a Gal4 negative control (see text for details). **D** Pie chart of the identified enhancers and suppressors of MM formation, resulting from *Smn* RNAi depletion using the Cg-Gal4 driver. See Table 1 for details.

co-depletion of *Rel* gave similar results to those obtained with *Rel* mutants (compare Figs. 5B, C).

Next, we tested the effects of co-depleting SMN complex proteins and other known associated factors; see Table 1 for a complete list. As shown, the knockdown of snRNP components (SmB, SmD1, SmD2, and SmE) and one SMN complex member, Gemin2 (Gem2), had little effect on melanotic mass number (Fig. 5D, Table 1). Co-depletion of two other SMN complex members, Gemin3 (Gem3; [61]), Gemin4 (Gaulos/Gem4a, Gem4b, Gem4c; [62]), and the arginine methyltransferase, Prmt5 (Art5/capsuleen; [63]), suppressed the melanization phenotype

Table 1 Summary of melanotic mass screening data

Genotype	Secondary Target				Statistics					
Smn-RNAi[JF02057] (FBgn0036641) plus:	Flybase Gene Id	Gene Symbol	Chr Loc	Modifier Type	N-value	Avg # MMs	SEM	P-value	Q-value	Comment
Oregon-R	–	–	–	–	50	0.18	0.09	7.9E-24	7.6E-23	Wildtype Control (no RNAi)
Cg-Gal4/+; Smn-RNAi[JF02057]/+	–	–	–	–	430	2.14	0.46	–	–	Smn-only RNAi Control
Cg-Gal4/+; Smn-RNAi[JF02057]/UAS:NLS-GFP	–	N/A	3	UAS	39	2.49	0.48	4.95E-01	5.53E-01	2' UAS Control
Cg-Gal4/+; Dif-RNAi[HM05257]/JF02057	FBgn0011274	Dif	3	dsRNA	40	0.05	0.03	1.29E-33	1.01E-31	
Cg-Gal4/+; Atg9-RNAi[JF02891]/JF02057	FBgn0034110	Atg9	3	dsRNA	50	0.10	0.05	4.98E-31	1.94E-29	Autophagy related
Cg-Gal4/+; shaggy-RNAi[JF01256]/JF02057	FBgn0003371	sgg	3	dsRNA	40	0.20	0.08	8.94E-25	2.32E-23	
Cg-Gal4/+; STAT-RNAi[HMS00035]/JF02057	FBgn0016917	Stat92E	3	dsRNA	46	0.26	0.08	4.87E-24	9.49E-23	
Cg-Gal4/+; Fimbrin-RNAi[HMS00729]/JF02057	FBgn0024238	Fim	3	dsRNA	50	0.34	0.08	7.17E-22	1.12E-20	Smn/SMA modifier
Cg-Gal4/+; p38a-RNAi[HMS01224]/JF02057	FBgn0015765	p38a	3	dsRNA	50	0.20	0.11	1.51E-21	1.88E-20	MAP kinase
Cg-Gal4/+; Art1[KG09631]/JF02057	FBgn0037834	Prmt1	3	mutation	67	0.21	0.14	1.68E-21	1.88E-20	
Cg-Gal4/+; Atg1-RNAi[HMS02750]/JF02057	FBgn0260945	Atg1	2	dsRNA	50	0.28	0.10	3.96E-21	3.86E-20	Autophagy related
Cg-Gal4/shaggy-RNAi[HMS01751]; JF02057/+	FBgn0003371	sgg	2	dsRNA	50	0.26	0.11	4.35E-20	3.77E-19	
Cg-Gal4/+; kayak-RNAi[HMS00254]/JF02057	FBgn0015765	kay	3	dsRNA	50	0.38	0.10	2.26E-19	1.76E-18	
Cg-Gal4/+; Relish-RNAi[HM05154]/JF02057	FBgn0014018	Rel	3	dsRNA	50	0.36	0.13	1.74E-16	1.23E-15	
Cg-Gal4/Gemin4-RNAi[HMJ22884]; JF02057/+	FBgn0029686	Gem4x	2	dsRNA	50	0.46	0.13	3.28E-15	2.13E-14	Targets Gem-4a,-4b,-4c (SMN partner)
Cg-Gal4/+; basket-RNAi[JF01275]/JF02057	FBgn0000229	bsk	3	dsRNA	41	0.56	0.12	2.29E-14	1.37E-13	
Cg-Gal4/+; p38a-RNAi[JF02625]/JF02057	FBgn0015765	p38a	3	dsRNA	50	0.40	0.15	1.24E-13	6.88E-13	MAP kinase
Cg-Gal4/+; cactus-RNAi[GL00627]/JF02057	FBgn0000250	cact	3	dsRNA	50	0.30	0.19	6.88E-12	3.58E-11	
Cg-Gal4/Art5[e00797]; JF02057/+	FBgn0015925	Prmt5	2	mutant	42	0.43	0.20	8.39E-10	4.09E-09	
Cg-Gal4/p38b-RNAi[JF03341]; JF02057+	FBgn0024846	p38b	2	dsRNA	50	0.56	0.20	9.11E-09	4.18E-08	MAP kinase
Cg-Gal4/+; Fimbrin-RNAi[HMS00937]/JF02057	FBgn0024238	Fim	3	dsRNA	39	0.59	0.20	2.25E-08	9.74E-08	Smn/SMA modifier
Cg-Gal4/+; Traf6[HMS00880]/JF02057	FBgn0265464	Traf6	3	dsRNA	50	0.60	0.21	4.09E-08	1.68E-07	
Cg-Gal4/Lsm10[f06616]; JF02057/+	FBgn0033554	Lsm10	2	mutation	50	0.52	0.23	6.12E-08	2.39E-07	U7 snRNP
Cg-Gal4/+; JF02057/Akt1-RNAi[HMS00007]	FBgn0033554	Akt	3	dsRNA	50	29.58	4.48	1.52E-07	5.63E-07	
Cg-Gal4/+; Gemin3[e03688]/JF02057	FBgn0011802	Gem3	3	mutation	50	0.70	0.22	3.93E-07	1.39E-06	SMN partner
Cg-Gal4/neurocalcin-RNAi[HMJ2153]; JF02057/+	FBgn0013303	Nca	2	dsRNA	43	0.81	0.22	3.58E-06	1.21E-05	Smn/SMA modifier
Traf6 EP1516-ex1/+; Cg-Gal4/+; JF02057/+	FBgn0265464	Traf6	X	mutation	92	0.98	0.20	4.18E-06	1.36E-05	
UAS-p38b.DN/+; Cg-Gal4/+; JF02057/+	FBgn0024846	p38b	X	UAS	44	0.68	0.28	1.87E-05	5.67E-05	Control – Dom Neg OE Tg
Cg-Gal4/+; Dif-RNAi[HM05191]/JF02057	FBgn0011274	Dif	3	dsRNA	50	0.80	0.25	1.89E-05	5.67E-05	
Cg-Gal4/+; Jra-RNAi[JF01184]JF02057	FBgn0001291	Jra	3	dsRNA	50	0.94	0.23	3.59E-05	1.04E-04	
Cg-Gal4/+; JMJD6-RNAi[HMC00576]/JF02057	FBgn0038948	JMJD6	3	dsRNA	50	4.76	0.60	9.35E-05	2.61E-04	
Cg-Gal4/+; Slmb-RNAi[HMS00946]/JF02057	FBgn0283468	slmb	3	dsRNA	45	1.02	0.23	9.89E-05	2.66E-04	
Cg-Gal4/Gemin4-RNAi[HMJ21393]; JF02057/+	FBgn0029686	Gem4a	2	dsRNA	50	1.06	0.29	1.59E-03	5.67E-05	Targets Gem4a/Glos only (SMN partner)
Cg-Gal4/+; Rel[KG07752]/JF02057	FBgn0014018	Rel	3	dsRNA	50	0.9	0.36	2.17E-03	3.99E-03	
Cg-Gal4/Lsm11[c02047]; JF02057/+	FBgn0033450	Lsm11	2	mutation	50	1.04	0.34	4.63E-03	5.29E-03	U7 snRNP
Cg-Gal4/+; Lst8-RNAi[HMS01350]/JF02057	FBgn0264691	Lst8	3	dsRNA	50	4.36	0.74	4.76E-03	1.09E-02	
Lst8[1]/+; Cg-Gal4/+; JF02057/+	FBgn0264691	Lst8	X	mutation	41	4.90	0.92	4.97E-03	1.09E-02	
Cg-Gal4/+; mTor-RNAi[HMS00904]/JF02057	FBgn0021796	mTor	3	dsRNA	43	0.67	0.29	1.46E-03	1.11E-02	S/T Kinase
Cg-Gal4/cactus[4]; JF02057/+	FBgn0000250	cact	2	mutation	50	0.96	0.42	1.10E-02	2.37E-02	
Cg-Gal4/+; bendless[JF03148]/JF02057	FBgn0000173	ben	3	dsRNA	50	1.28	0.29	1.12E-02	2.37E-02	
Cg-Gal4/+; Art1-RNAi[JF001306]/JF02057	FBgn0037834	Prmt1	3	dsRNA	50	3.38	0.45	1.17E-02	2.41E-02	
Cg-Gal4/+; Gemin3[rL562]/JF02057	FBgn0011802	Gem3	3	mutation	50	1.28	0.31	1.65E-02	3.29E-02	SMN partner
Cg-Gal4/+; neurocalcin-RNAi[JF03398]/JF02057	FBgn0013303	Nca	3	dsRNA	47	1.19	0.39	2.67E-02	5.21E-02	Smn/SMA modifier
Cg-Gal4/+; TAK-RNAi[HMS00282]/JF02057	FBgn0026323	Tak1	3	dsRNA	41	1.15	0.41	2.88E-02	5.28E-02	
Cg-Gal4/+; hopscotch-RNAi[HMS00761]/JF02057	FBgn0004864	hop	3	dsRNA	50	1.30	0.34	2.90E-02	5.28E-02	
Cg-Gal4/+; Atg1-RNAi[JF02273]/JF02057	FBgn0260945	Atg1	3	dsRNA	50	1.12	0.43	2.91E-02	5.28E-02	Autophagy related
Cg-Gal4/+; Gemin2-RNAi[HMS01355]/JF02057	FBgn0036850	Gem2	3	dsRNA	50	1.54	0.29	7.01E-02	1.24E-01	SMN partner
Cg-Gal4/+; Relish-RNAi[HMS00070]/JF02057	FBgn0014018	Rel	3	dsRNA	46	1.13	0.53	7.48E-02	1.30E-01	
Cg-Gal4/dorsal[4]; JF02057/+	FBgn0260632	dl	2	mutation	50	1.28	0.45	7.82E-02	1.33E-01	
Cg-Gal4/Thor[2]; JF02057/+	FBgn0261560	Thor	2	mutation	50	1.42	0.38	8.24E-02	1.37E-01	
Cg-Gal4/+; Slmb-RNAi[HMS00838]/JF02057	FBgn0283468	slmb	3	dsRNA	46	5.67	2.10	9.95E-02	1.62E-01	
Cg-Gal4/UAS-dorsal.H; JF02057/+	FBgn0260632	dl	2	UAS	36	3.86	1.03	1.07E-01	1.71E-01	Control – WT Overexpressor Tg
Cg-Gal4/+; SmD1[SH003]/JF02057	FBgn0261933	SmD1	3	mutation	50	1.40	0.49	1.55E-01	2.37E-01	Spliceosomal snRNP
Cg-Gal4/+; Akt1[04226]/JF02057	FBgn0033554	Akt	3	dsRNA	50	1.22	0.62	1.55E-01	2.37E-01	Weak hypomorph
Cg-Gal4/+; ref(2)P-RNAi[HMS00958]/JF02057	FBgn0003231	ref(2)P	3	dsRNA	50	3.52	1.07	2.09E-01	3.13E-01	
Cg-Gal4/+; dorsal-RNAi[HMS00028]/JF02057	FBgn0260632	dl	3	dsRNA	50	1.48	0.52	2.28E-01	3.36E-01	
Cg-Gal4/+; TSC1-RNAi[HMC03672]/JF02057	FBgn0026317	Tsc1	3	dsRNA	50	2.86	0.70	3.19E-01	4.61E-01	
Cg-Gal4/+; Thor-RNAi[HMS01555]/JF02057	FBgn0261560	Thor	3	dsRNA	42	2.95	0.85	3.49E-01	4.96E-01	
Cg-Gal4/TSC1-RNAi[HMJ21477]; JF02057/+	FBgn0026317	Tsc1	2	dsRNA	45	2.73	0.62	3.58E-01	4.98E-01	
Cg-Gal4/ref(2)P[KG0926]; JF02057/+	FBgn0003231	ref(2)P	2	mutation	50	2.84	0.76	3.71E-01	5.08E-01	
Traf6[G904]/+;Cg-Gal4/+; JF02057/+	FBgn0265464	Traf6	X	mutation	50	1.86	0.37	4.96E-01	6.67E-01	Control – misexpression element
Cg-Gal4/+; SmD1[e02855]/JF02057	FBgn0261933	SmD1	3	mutation	50	2.50	0.55	5.29E-01	7.00E-01	Spliceosomal snRNP
Cg-Gal4/SmB[SNRPB]; JF02057/+	FBgn0262601	SmB	2	mutation	41	2.39	0.79	7.55E-01	9.76E-01	Spliceosomal snRNP
Cg-Gal4/SmE[SNRPE]; JF02057/+	FBgn0261790	SmE	2	mutation	50	2.28	0.45	7.67E-01	9.76E-01	Spliceosomal snRNP
Cg-Gal4/Art5[RM50]; JF02057/+	FBgn0015925	Prmt5	2	mutation	43	1.84	1.04	7.76E-01	9.76E-01	Negative control allele
Cg-Gal4/+; SmD2[EY3399]/JF02057	FBgn0261789	SmD2	3	mutation	50	2.22	0.51	8.76E-01	1.00E+00	Spliceosomal snRNP
Cg-Gal4/+; TSC2-RNAi[HM04083]/JF02057	FBgn0005198	gig	3	dsRNA	41	2.15	0.63	9.89E-01	1.00E+00	

(Fig. 5D). Interestingly, Gem3 and Gem4 were both previously shown to form complexes in S2 cells with the immune deficiency (imd) protein [64], suggesting a potential role for Gemin subcomplexes in immune signaling. Prmt5 is a notable suppressor not only because knockdown of its corresponding arginine demethylase (JMJD6) enhanced the number of melanotic masses (Fig. 5D, Table 1), but also because the Tudor domain of SMN is known to bind to dimethylated targets of Prmt5 [65, 66]. We previously showed that complete loss of *Drosophila* Prmt5 function has little effect on organismal viability or snRNP assembly [63, 67]. Collectively, these data indicate that the presumptive SMN-interacting, innate immune signaling target of Prmt5 and JMJD6 is

unlikely to be connected to SMN's role in spliceosomal snRNP biogenesis. We therefore sought to test other candidate signaling factors that interact with SMN.

A common feature of the Toll (Toll), IMD (PGRP), and TNF/Eiger (Wgn) signaling pathways (Fig. 5A) is a protein complex that forms a platform for K63-linked ubiquitylation and recruitment of downstream factors like Tak1 (TGF-β activated kinase 1), Tab2 (TAK1-associated binding protein 2), and key (kenny, a.k.a. NEMO). Analogous complexes function within the mammalian TLR (Toll-like receptor) and TNFa (tumor necrosis factor alpha) signaling cascades [68–71]. In mammals, TLR signaling involves the E3 ligase Traf6 (TNF Receptor Associated Factor 6), whereas TNFa signaling utilizes Traf2 [70, 72, 73]. In flies, a single protein, called Traf6/dTRAF2, performs both functions [68, 74]. As in humans, fly Traf6 functions together with the E2 conjugating enzyme Ubc13/bendless [70]. Ubc13/bendless (Ben) and the Ubiquitin-conjugating enzyme variant 1A (Uev1A) activate Tak1, a downstream kinase in the IMD pathway, although Traf6 appears to be dispensable for this activation, at least in S2 cells [75, 76].

Intriguingly, human TRAF6 was shown to co-precipitate with SMN [77]. The authors hypothesized that SMN might serve as a negative regulator of NF-kB signaling, although the effect could be indirect [77]. We therefore tested this idea in vitro with purified components and found that human GST-TRAF6 interacts directly with the SMN•Gem2 heterodimer (Fig. S2A). Experiments aimed at determining if this biochemical interaction was conserved in the fly were inconclusively negative. Transgenic overexpression of Flag-tagged fruit fly Traf6 (tub-Gal4 > UAS:Flag-Traf6) failed to co-immunoprecipitate endogenous SMN (Fig. S2B). As measured by AP-MS (affinity purification followed by mass spectrometry), we failed to detect *Drosophila* Traf6 in co-precipitates from embryonic lysates expressing Flag-SMN as the sole source of SMN protein. However, the same Flag-SMN pulldowns identified the E2 conjugase and Traf6 binding partner, Ubc13/Ben [19].

Given that biologically important interactions are not necessarily biochemically stable enough to withstand a pulldown assay, we decided to test *bendless* (*ben*) and *Traf6* by genetic interaction in the larval melanization assay. As shown in Fig. 5, a reduction in dosage of either *Traf6* or *ben* resulted in a significant decrease in the number of melanotic masses per animal, compared to that of the SMN RNAi-only control. In summary, these observations show that Toll, IMD, and TNF-Eiger signaling pathways are disrupted following the loss of SMN expression within the immune system (fat body and hemocytes), leading to the formation of melanotic masses in fly models of SMA.

Discussion

Our multi-omic investigation of fly models of SMA supports a role for dysregulated innate immunity in the peripheral pathophysiology associated with the disease in humans. The molecular signatures of an activated immune response were readily apparent in the whole-animal transcriptomes and proteomes of two hypomorphic *Smn* mutants. Moreover, we observed aberrant immune activation in all SMA models examined, including very mild models (Fig. 3) that do not display viability or neuromuscular defects during larval stages [20]. Furthermore, the degree of immune activation (Fig. 3), as measured by larval melanotic mass formation, correlated well with phenotypic class of the mutations [20]. That is, Class 2 SMA alleles had the most melanotic masses, Class 4 the fewest, and Class 3 had an intermediate number (Fig. 3E). These results are notably consistent with recent findings of immune dysregulation in mammalian models of SMA and in pediatric SMA patients [31–36, 78, 79]. Furthermore, our work suggests that this conserved dysregulation of innate signaling is a primary effect of SMN loss in immune cells and tissues (e.g., the hemolymph) rather than a secondary consequence of SMN loss elsewhere.

Neurodegeneration and the sustained activation of innate immunity

The extent to which the dysregulation of immune systems contributes to neuroinflammation and neuromuscular degeneration in SMA remains to be determined. Emerging evidence suggests that hyperactivation of innate immunity is a common feature of neurological disease. Our finding that downstream targets of NF-kB like transcription factors are upregulated in *Smn* hypomorphs is particularly revealing. However, one limitation of the study is that the proteomics do not implicate a clear 'smoking gun' signature regarding specific upstream factors that are activated by reduced levels of SMN. Most notable among the differentially expressed upstream factors are GNBP3 and imd itself (Fig. 2). Given that both Gem3 and Gem4 were hits in the screen (Fig. 5) and have been shown to co-purify with imd protein [64], it seems that other members of the SMN complex may also play a role in innate immunity.

Signaling factors are often activated by PTMs that do not necessarily result in a change in overall protein levels (e.g., kinases or regulatory proteases). Our TMT-MS approach is unable to identify such changes. Alternatively, upstream factors other than Dap-type proteoglycans could bypass the top of the pathway and impinge on it downstream. For example, there may be extracellular or intracellular DAMPs (damage-associated molecular

patterns) that serve to activate Toll and/or Imd pathways in *Smn* mutants (Fig. 5A). Interestingly, the V72G mutant proteome displayed altered levels of several known SMA disease modifiers: CG17931/Serf, coronin (coro), and Zinc finger protein 1 (Zpr1); see Table S1 [80–85].

Cytosolic nucleic acid sensors serve as critical elements of innate immunity in many different organisms, reviewed in [86]. In mammalian cells, two of the aforementioned SMA modifiers (CORO1C and ZPR1) have been implicated in R-loop resolution and the subsequent DNA-damage response [87–89], both of which fall into the general category of DAMPs. Zpr1 is notable for its previously reported physical interactions with SMN and nucleocytoplasmic import proteins [90, 91]. The proteomes of both T205I and V72G mutants display additional evidence of a DNA-damage response (Table S1). Importantly, cytoplasmic R-loop accumulation and DNA-damage response factors were recently linked to the activation of innate immunity via the Toll-like receptor and the cGAS-STING (cyclic GMP-AMP Synthase—Stimulator of Interferon Response Genes) pathway [92].

In *Drosophila*, cGAS-Sting signaling is conserved [93–95] but is thought to bypass interferon regulatory factor 3 (IRF3) and directly activate NF-kB signaling via Relish and trigger an autophagic response [86, 96–98]. Notably, we also found Atg7 was upregulated in V72G animals (Table S3), but RNAi for the p62 ortholog, ref(2)p, had no effect in our larval melanization screen (Fig. 5). Unfortunately, proteomic analysis of whole-larvae does not allow us to identify the tissues in which the various proteins may be differentially expressed. However, our finding that all three NF-kB-like proteins are upregulated in SMA model flies indicates a widespread and ongoing activation of immune signaling.

Sustained overexpression of NF-kB-like proteins is thought to contribute to disease progression in a variety of neurological disorders, including Alzheimer's disease [99, 100], amyotrophic lateral sclerosis [101–105], ataxia-telangiectasia [106, 107], polyglutamine disorders [108], and retinal degeneration [109]. The consequences of sustained activation of NF-kB via cGAS-Sting and its potential contribution to neurodegeneration and/or neurodevelopment remain to be determined [110, 111]. Additional studies will be required to determine if there is an etiological connection between the observed hyperimmune activation and the neuromuscular dysfunction in humans and animal models of SMA.

SMN, K63-linked polyubiquitylation, and immune signaling networks

In mammals and flies, the TLR/Toll and TNF/IMD signaling pathways function through analogous enzymatic cascades and complexes (Fig. 5A). Prominently featured in these pathways are receptor-proximal adaptor proteins (e.g., mammalian RIP1 or fly imd) that are activated by K63-linked ubiquitylation (K63-Ub) [59, 112, 113]. The protein complex that carries out these crucial post-translational modifications includes the E2 conjugating enzymes and cofactors Ubc13/bendless (Ben), Uev1a, and Ubc5/effete, along with two other RING-domain E3 ligases, Diap2 or Traf6 (see Fig. 5A). The presence of these K63-Ub oligomers triggers binding of Tab2 and key, leading to activation of the downstream kinase Tak1. Although the precise molecular details are uncertain [114], Traf6 likely plays both enzymatic and structural roles in this process [68, 75, 115, 116].

Tak1 phosphorylation of I-kappaB kinase, mediated by binding Tab2 and key, leads to translocation of NF-kB transcription factors to the nucleus, and expression of antimicrobial peptide (AMP) genes (Fig. 5A). Traf6, Diap2, and Ben thus constitute an evolutionarily conserved node or nexus through which multiple intracellular signaling pathways are connected (box in Fig. 5A). The work here identifies SMN as a negative regulator of this complex, supported by both biochemical (Fig. S2A, [19, 77]) and genetic (Fig. 5A–B) interactions. In summary, we show that partial loss of SMN function (either by mutation or depletion) results in the sustained activation of innate immunity.

Conclusions

Our proteomic analyses of mild and intermediate fly models of SMA reveal clear signatures of an immune response in the absence of an external challenge. These include, but are not limited to, overexpression of AMPs (Figs. 1 and 2). Notably, Ganetzky and colleagues have shown that ectopic expression of individual AMP genes can bypass this immune signaling cascade and cause disease, as the neural overexpression of AMP transgenes is sufficient to cause neurodegeneration in the fly brain [117]. Although the precise mechanisms remain unclear, neuroinflammatory responses like those identified here are likely to contribute to the pathophysiology of neurodegenerative diseases like Spinal Muscular Atrophy.

Methods

Drosophila strains and husbandry

Fly stocks were maintained on molasses and agar at room temperature (25 °C) in vials or half-pint bottles. As previously described, FLAG-Smn^{Tg} transgenes were site-specifically integrated into a PhiC31 landing site (86Fb) that had been recombined into the Smn^{X7} null background [17]. The Smn^{X7} null line was a gift of S. Artavanis-Tsakonis (Harvard University, Cambridge, USA). C15-GAL4 [53] was a gift of A. Frank, University of Iowa (Iowa City, USA). All other GAL4/*UAS-RNAi* stocks were obtained

from the Bloomington Drosophila Stock Center (BDSC); see Table 1 for details.

To generate larvae expressing a single *Smn* missense mutant allele, Smn^{X7}/TM6B-GFP virgin females were crossed to Smn^{X7}, Smn^{Tg}/TM6B-GFP males at 25 °C. To reduce stress from overpopulation and/or competition from heterozygous siblings, crosses were performed on molasses plates with yeast paste, and GFP negative (Smn^{X7}, Smn^{Tg}/Smn^{X7}) larvae were sorted into vials containing molasses fly food during the second instar larval stage. Sorted larvae were raised at 25 °C until the desired developmental stage was reached.

Experiments involving *UAS-Smn-RNAi* expression were carried out at 29 °C to maximize expression from the GAL4/*UAS* system and, therefore, the degree of *Smn* knockdown. To maintain consistency across experiments, we used molasses plates with yeast paste and subsequent sorting for all *Smn-RNAi* experiments.

Tandem mass tag (TMT) sample preparation

Cell lysates (100 µg; $n=3$) were lysed in 8 M urea, 75 mM NaCl, 50 mM Tris, pH 8.5; reduced with 5 mM DTT for 45 min at 37 °C; and alkylated with 15 mM iodoacetamide for 30 min in the dark at room temperature. Samples were digested with LysC (Wako, 1:50 w/w) for 2 h at 37 °C, then diluted to 1 M urea and digested with trypsin (Promega, 1:50 w/w) overnight at 37 °C. The resulting peptide samples were acidified to 0.5% trifluoracetic acid, desalted using desalting spin columns (Thermo), and the eluates were dried via vacuum centrifugation. Peptide concentration was determined using Quantitative Colorimetric Peptide Assay (Pierce).

Samples were labeled with TMT10plex (Thermo Fisher). 40 µg of each sample was reconstituted with 50 mM HEPES pH 8.5, then individually labeled with 100 µg of TMT reagent for 1 h at room temperature. Prior to quenching, the labeling efficiency was evaluated by LC–MS/MS (liquid chromatography and tandem mass spectrometry) analysis of a pooled sample consisting of 1 ul of each sample. After confirming > 98% efficiency, samples were quenched with 50% hydroxylamine to a final concentration of 0.4%. Labeled peptide samples were combined 1:1, desalted using Thermo desalting spin column, and dried via vacuum centrifugation. The dried TMT-labeled sample was fractionated using high pH reversed phase HPLC [118]. Briefly, the samples were offline fractionated over a 90-min run, into 96 fractions by high pH reverse-phase HPLC (Agilent 1260) using an Agilent Zorbax 300 Extend-C18 column (3.5-µm, 4.6 × 250 mm) with mobile phase A containing 4.5 mM ammonium formate (pH 10) in 2% (vol/vol) LC–MS grade acetonitrile, and mobile phase B containing 4.5 mM ammonium formate (pH 10) in 90% (vol/vol) LC–MS grade acetonitrile. The 96 resulting fractions were then concatenated in a non-continuous manner into twenty-four fractions and dried down via vacuum centrifugation and stored at − 80 °C until further analysis.

Liquid chromatography-tandem mass spectrometry (LC–MS/MS)

Twenty-four proteome fractions were analyzed by LC–MS/MS using an Easy nLC 1200 coupled to an Orbitrap Fusion Lumos Tribrid mass spectrometer (Thermo Scientific). Samples were injected onto an Easy Spray PepMap C18 column (75 µm id × 25 cm, 2 µm particle size) (Thermo Scientific) and separated over a 120-min method. The gradient for separation consisted of 5–42% mobile phase B at a 250 nl/min flow rate, where mobile phase A was 0.1% formic acid in water and mobile phase B consisted of 0.1% formic acid in 80% ACN.

For the proteome fractions, the Lumos was operated in SPS-MS3 mode [119], with a 3-s cycle time. Resolution for the precursor scan (m/z 350–2000) was set to 120,000 with a AGC target set to standard and a maximum injection time of 50 ms. MS2 scans consisted of CID normalized collision energy (NCE) 30; AGC target set to standard; maximum injection time of 50 ms; isolation window of 0.7 Da. Following MS2 acquisition, MS3 spectra were collected in SPS mode (10 scans per outcome); HCD set to 65; resolution set to 50,000; scan range set to 100–500; AGC target set to 200% with a 150 ms maximum inject time.

TMT data analysis

TMT proteome RAW files were processed using Proteome Discoverer version 2.5. "TMT10" was used as the quantitation method. Peak lists were searched against a reviewed Uniprot drosophila database (downloaded Feb 2020 containing 21,973 sequences), appended with a common contaminants database, using Sequest HT within Proteome Discoverer. Data were searched with up to two missed trypsin cleavage sites and fixed modifications were set to TMT peptide N-terminus and Lys and carbamidomethyl Cys. Dynamic modifications were set to N-terminal protein acetyl and oxidation Met. Quantitation was set to MS3, precursor mass tolerance was set to 10 ppm, and fragment mass tolerance was set to 0.5 Da. Peptide false discovery rate was set to 1%. Reporter abundance based on intensity, SPS mass matches threshold set to 50, and razor and unique peptides were used for quantitation.

Statistical analysis was performed within Proteome Discoverer (version 2.4). Benjamini–Hochberg corrected p-values (q-values) were calculated for each pairwise comparison, and statistical significance is defined as q-value < 0.05. Log2 fold change (FC) ratios

were calculated using the averaged normalized TMT intensities.

For Gene Ontology (GO) analysis, Uniprot protein IDs were converted to Flybase Gene IDs and gene symbols. GO enrichment was performed with FlyEnrichr, using the GO Biological Process (BP) category from AutoRIF [120, 121].

Transcriptome profiling

RNA-seq analysis was performed on previously published datasets, retrieved as fastq files from the NCBI Gene Expression Omnibus (GEO). GEO accession numbers used here were as follows: GSE49587, GSE81121, and GSE138183. Alignments of paired-end reads were performed with HISAT2 and Ensemble release 109 of the *Drosophila melanogaster* genome (BDGP6.32) [122, 123]. Differential expression of transcripts was performed with kallisto and sleuth [44, 45]. For the determination of transcript abundance, the number of bootstrap samples was set at 100. StringTie and DESeq2 were used to determine differential gene expression [124, 125].

Scoring melanotic masses

Wandering third instar larvae were removed from vials, washed briefly in a room temperature water bath, dried, and placed on an agar plate under white light and 2× magnification. When melanotic masses were identified in a larva, both the size of the largest mass (size score) and the total number of masses (mass score) were qualitatively determined. Size scoring used the following criteria: small masses range in size from barely visible specks to smooth round dots with a diameter no more than 1/10th the width of the larva; medium masses range from anything larger than a small mass to those with a diameter up to 1/3 the larval width; large masses had a diameter greater than or equal to 1/3 the larval width. Larvae were manipulated to allow for observation of all sides/regions; observation was performed for at least 20 s in all cases.

Statistical analysis

GraphPad Prism version 7 was used to calculate *p*-values for comparison of melanotic masses, using a one-way ANOVA with a Dunnet correction for multiple comparisons.

Protein–protein interactions

In vitro binding and co-immunoprecipitation (co-IP) assays were performed as previously described [19]. Briefly, GST and GST-hTRAF6 were purified from *E. coli*, strain BL21*. Bacteria were grown at 37 °C overnight and then induced using 1 mM isopropyl-β-d-thiogalactopyranoside (IPTG). Recombinant protein was extracted and purified using glutathione sepharose 4B beads. SMN•Gem2 complexes were co-expressed in *E. coli* as described [126]. For the anti-Flag pulldown assays, transgenic flies exclusively expressing Flag-dSMN from the native *Smn* promoter [19] or animals co-expressing a *UAS:Flag-dTraf6* transgene (Bloomington stock #82,150) and a *tubulin*-Gal4 driver line were used to carry out co-IP assays [19]. Following the pulldowns, co-purified proteins were eluted and run on an SDS–PAGE gel for Western blotting [19].

Supplementary Information

The online version contains supplementary material available at https://doi.org/10.1186/s12915-024-01888-z.

Additional file 1: Table S1–S3.

Additional file 2: Table S4–S5.

Additional file 3: Table S6–S10.

Additional file 4: Table S11.

Additional file 5: Table S12-S13.

Additional file 6: Figure S1. Isoform-specific differences in *Smn* mutants versus controls. **A)** Volcano plot of differentially expressed transcripts in *Smn* null animals. Transcripts associated with innate immunity are indicated with red circles and a subset of those are labeled with transcript symbols for the specific mRNA isoform difference. The axes correspond to: a Benjamini-Hochberg (False Discovery Rate (FDR) < 0.05) adjusted *p*-value (qval) and a Wald test-derived representation of a normalized fold change (beta factor). **B)** The heat map displays the respective mean transcripts per million reads for the different genotypes used in (A). The values are scaled and normalized per row (z-score). The heat map shows approximately half of the differentially expressed transcripts from (A). **C)** Scatter plot comparison of isoform-specific protein changes identified in the V72G proteome versus isoform-specific RNA changes found in the *Smn* null transcriptome. RNA and proteins associated with innate immunity are represented with larger dots and labeled. **Figure S2.** Evaluation of protein–protein interactions. **A)** GST-pulldown experiment using recombinant human SMN•Gem2 [22] and GST-TRAF6. GST and GST-TRAF6 were expressed in E.coli and purified using anti-Glutathione beads. Pulldown assays were performed and analyzed by western blotting with either anti-hSMN (top) or anti-GST (bottom) antibodies. As shown, GST-hTRAF6 interacts directly with human SMN•Gem2. **B)** Flag-pulldown experiment using lysates from tub-Gal4 > UAS:Flag-dTraf6 animals (Flag-Traf6) or from control animals bearing a *Flag-Smn* transgene [18] as the only source of SMN protein (Flag-SMN). Inputs are on the left and proteins eluted from the Flag beads following pulldowns are on the right. As shown, Flag-SMN co-purifies with itself in the control lysates but Flag-Traf6 fails to pull down endogenous dSMN in the experimental cross.

Acknowledgements

We thank E.C. Garcia for helpful discussions, V. Vandadi for assistance with figure preparation, and the Bloomington Drosophila Stock Center for providing fly strains. We are deeply indebted to D.A. Harrison for providing research space to ELG during the preparation of the manuscript.

Data sharing

Proteomic data are available via the ProteomeXchange with identifier PXD046801.

Authors' contributions

All authors have read and approved the manuscript. AMS and AGM conceived and designed the study; AMS, EJG, ACR, RES, and LEH were involved in data acquisition and analysis; EJG, AGM, and AMS interpreted the data; AGM and EJG wrote the first draft; AGM, EJG, and AMS revised the manuscript.

Funding
This work was supported by the US National Institutes of Health, grant R35-GM136435 (to AGM).

Availability of data and materials
All *Drosophila* stocks are available upon request. The authors affirm that all data necessary for confirming the conclusions of the article are present within the article, figures, and tables. The tandem mass spectrometry labeling data have been deposited to the ProteomeXchange Consortium via the PRIDE partner repository [127] using the dataset identifier PXD046801.

Declarations

Ethics approval and consent to participate
Not applicable; there are no human subjects or vertebrate animals involved in this study.

Competing interests
The authors declare that they have no competing interests.

Author details
[1]Integrative Program for Biological and Genome Sciences, University of North Carolina at Chapel Hill, Chapel Hill, NC 27599, USA. [2]Department of Biology, University of Kentucky, Lexington, KY, USA. [3]Curriculum in Genetics and Molecular Biology, University of North Carolina at Chapel Hill, Chapel Hill 27599, USA. [4]Department of Pharmacology, University of North Carolina at Chapel Hill, Chapel Hill, USA. [5]Department of Biology, University of North Carolina at Chapel Hill, Chapel Hill 27599, USA. [6]Department of Genetics, University of North Carolina at Chapel Hill, Chapel Hill 27599, USA. [7]RNA Discovery and Lineberger Comprehensive Cancer Centers, University of North Carolina at Chapel Hill, Chapel Hill 27599, USA. [8]Department of Biology, University of North Carolina at Greensboro, Greensboro, NC 27402, USA. [9]Present Address: Lake, Erie College of Osteopathic Medicine, Bradenton, FL, USA. [10]Present Address, Radford University, Radford, VA, USA.

Received: 28 October 2023 Accepted: 16 April 2024
Published online: 25 April 2024

References

1. Lefebvre S, Burglen L, Reboullet S, Clermont O, Burlet P, Viollet L, Benichou B, Cruaud C, Millasseau P, Zeviani M, et al. Identification and characterization of a spinal muscular atrophy-determining gene. Cell. 1995;80(1):155–65.
2. O'Hern P, Garcia EL, Hao LT, Hart AC, Matera AG, Beattie CE. Nonmammalian animal models of spinal muscular atrophy. In: Sumner CJ, Paushkin S, Ko CP, editors. Spinal muscular atrophy: disease mechanisms and therapy. Academic; 2017. p. 221–39.
3. Lefebvre S, Burlet P, Liu Q, Bertrandy S, Clermont O, Munnich A, Dreyfuss G, Melki J. Correlation between severity and SMN protein level in spinal muscular atrophy. Nat Genet. 1997;16(3):265–9.
4. Wirth B. An update of the mutation spectrum of the survival motor neuron gene (SMN1) in autosomal recessive spinal muscular atrophy (SMA). Hum Mutat. 2000;15(3):228–37.
5. Kugelberg E, Welander L. Heredofamilial juvenile muscular atrophy simulating muscular dystrophy. AMA Arch Neurol Psych. 1956;75(5):500–9.
6. Dubowitz V: Sixty years of spinal muscular atrophy: a personal odyssey. In: Sumner CJ, Paushkin S, Ko C. Spinal muscular atrophy disease mechanisms and therapy. 2016. pp. xvii-xxi.
7. Mercuri E, Sumner CJ, Muntoni F, Darras BT, Finkel RS. Spinal muscular atrophy. Nat Rev Dis Primers. 2022;8(1):52.
8. Nishio H, Niba ETE, Saito T, Okamoto K, Takeshima Y, Awano H: Spinal muscular atrophy: the past, present, and future of diagnosis and treatment. Int J Mol Sci. 2023;24(15):11939.
9. Jablonka S, Schrank B, Kralewski M, Rossoll W, Sendtner M. Reduced survival motor neuron (Smn) gene dose in mice leads to motor neuron degeneration: an animal model for spinal muscular atrophy type III. Hum Mol Genet. 2000;9(3):341–6.
10. Gladman JT, Bebee TW, Edwards C, Wang X, Sahenk Z, Rich MM, Chandler DS. A humanized Smn gene containing the SMN2 nucleotide alteration in exon 7 mimics SMN2 splicing and the SMA disease phenotype. Hum Mol Genet. 2010;19(21):4239–52.
11. Osborne M, Gomez D, Feng Z, McEwen C, Beltran J, Cirillo K, El-Khodor B, Lin MY, Li Y, Knowlton WM, et al. Characterization of behavioral and neuromuscular junction phenotypes in a novel allelic series of SMA mouse models. Hum Mol Genet. 2012;21(20):4431–47.
12. Schrank B, Gotz R, Gunnersen JM, Ure JM, Toyka KV, Smith AG, Sendtner M. Inactivation of the survival motor neuron gene, a candidate gene for human spinal muscular atrophy, leads to massive cell death in early mouse embryos. Proc Natl Acad Sci USA. 1997;94(18):9920–5.
13. Hsieh-Li HM, Chang JG, Jong YJ, Wu MH, Wang NM, Tsai CH, Li H. A mouse model for spinal muscular atrophy. Nat Genet. 2000;24(1):66–70.
14. Monani UR, Sendtner M, Coovert DD, Parsons DW, Andreassi C, Le TT, Jablonka S, Schrank B, Rossoll W, Prior TW, et al. The human centromeric survival motor neuron gene (SMN2) rescues embryonic lethality in Smn(-/-) mice and results in a mouse with spinal muscular atrophy. Hum Mol Genet. 2000;9(3):333–9.
15. Le TT, Pham LT, Butchbach ME, Zhang HL, Monani UR, Coovert DD, Gavrilina TO, Xing L, Bassell GJ, Burghes AH. SMNDelta7, the major product of the centromeric survival motor neuron (SMN2) gene, extends survival in mice with spinal muscular atrophy and associates with full-length SMN. Hum Mol Genet. 2005;14(6):845–57.
16. Praveen K, Wen Y, Matera AG. A Drosophila model of spinal muscular atrophy uncouples snRNP biogenesis functions of survival motor neuron from locomotion and viability defects. Cell Rep. 2012;1(6):624–31.
17. Praveen K, Wen Y, Gray KM, Noto JJ, Patlolla AR, Van Duyne GD, Matera AG. SMA-causing missense mutations in survival motor neuron (Smn) display a wide range of phenotypes when modeled in Drosophila. PLoS Genet. 2014;10(8):e1004489.
18. Garcia EL, Wen Y, Praveen K, Matera AG. Transcriptomic comparison of Drosophila snRNP biogenesis mutants reveals mutant-specific changes in pre-mRNA processing: implications for spinal muscular atrophy. RNA. 2016;22(8):1215–27.
19. Gray KM, Kaifer KA, Baillat D, Wen Y, Bonacci TR, Ebert AD, Raimer AC, Spring AM, Have ST, Glascock JJ, et al. Self-oligomerization regulates stability of survival motor neuron protein isoforms by sequestering an SCF(Slmb) degron. Mol Biol Cell. 2018;29(2):96–110.
20. Spring AM, Raimer AC, Hamilton CD, Schillinger MJ, Matera AG. Comprehensive modeling of spinal muscular atrophy in Drosophila melanogaster. Front Mol Neurosci. 2019;12:113.
21. Raimer AC, Singh SS, Edula MR, Paris-Davila T, Vandadi V, Spring AM, Matera AG: Temperature-sensitive spinal muscular atrophy-causing point mutations lead to SMN instability, locomotor defects and premature lethality in Drosophila. Dis Model Mech. 2020;13(5):dmm043307.
22. Gupta K, Wen Y, Ninan NS, Raimer AC, Sharp R, Spring AM, Sarachan KL, Johnson MC, Van Duyne GD, Matera AG. Assembly of higher-order SMN oligomers is essential for metazoan viability and requires an exposed structural motif present in the YG zipper dimer. Nucleic Acids Res. 2021;49(13):7644–64.
23. Chan YB, Miguel-Aliaga I, Franks C, Thomas N, Trulzsch B, Sattelle DB, Davies KE, van den Heuvel M. Neuromuscular defects in a Drosophila survival motor neuron gene mutant. Hum Mol Genet. 2003;12(12):1367–76.
24. Chang HC, Dimlich DN, Yokokura T, Mukherjee A, Kankel MW, Sen A, Sridhar V, Fulga TA, Hart AC, Van Vactor D, et al. Modeling spinal muscular atrophy in Drosophila. PLoS ONE. 2008;3(9):e3209.
25. Rajendra TK, Gonsalvez GB, Walker MP, Shpargel KB, Salz HK, Matera AG. A Drosophila melanogaster model of spinal muscular atrophy reveals a function for SMN in striated muscle. J Cell Biol. 2007;176(6):831–41.
26. Imlach WL, Beck ES, Choi BJ, Lotti F, Pellizzoni L, McCabe BD. SMN is required for sensory-motor circuit function in Drosophila. Cell. 2012;151(2):427–39.
27. Garcia EL, Lu Z, Meers MP, Praveen K, Matera AG. Developmental arrest of Drosophila survival motor neuron (Smn) mutants accounts for differences in expression of minor intron-containing genes. RNA. 2013;19(11):1510–6.
28. Matera AG, Wang Z. A day in the life of the spliceosome. Nat Rev Mol Cell Biol. 2014;15(2):108–21.

29. Ohno M, Segref A, Bachi A, Wilm M, Mattaj IW. PHAX, a mediator of U snRNA nuclear export whose activity is regulated by phosphorylation. Cell. 2000;101(2):187–98.
30. Garcia EL: Allele-specific alternative splicing of Drosophila Ribosomal protein S21 suppresses a lethal mutation in the Phosphorylated adaptor for RNA export (Phax) gene. G3 (Bethesda). 2022;12(9):jkac195.
31. Deguise MO, De Repentigny Y, McFall E, Auclair N, Sad S, Kothary R. Immune dysregulation may contribute to disease pathogenesis in spinal muscular atrophy mice. Hum Mol Genet. 2017;26(4):801–19.
32. Deguise MO, Kothary R. New insights into SMA pathogenesis: immune dysfunction and neuroinflammation. Ann Clin Transl Neurol. 2017;4(7):522–30.
33. Khairallah MT, Astroski J, Custer SK, Androphy EJ, Franklin CL, Lorson CL. SMN deficiency negatively impacts red pulp macrophages and spleen development in mouse models of spinal muscular atrophy. Hum Mol Genet. 2017;26(5):932–41.
34. Thomson AK, Somers E, Powis RA, Shorrock HK, Murphy K, Swoboda KJ, Gillingwater TH, Parson SH. Survival of motor neurone protein is required for normal postnatal development of the spleen. J Anat. 2017;230(2):337–46.
35. Bonanno S, Cavalcante P, Salvi E, Giagnorio E, Malacarne C, Cattaneo M, Andreetta F, Venerando A, Pensato V, Gellera C, et al. Identification of a cytokine profile in serum and cerebrospinal fluid of pediatric and adult spinal muscular atrophy patients and its modulation upon nusinersen treatment. Front Cell Neurosci. 2022;16:982760.
36. Nuzzo T, Russo R, Errico F, D'Amico A, Tewelde AG, Valletta M, Hassan A, Tosi M, Panicucci C, Bruno C, et al. Nusinersen mitigates neuroinflammation in severe spinal muscular atrophy patients. Commun Med (Lond). 2023;3(1):28.
37. Brahms H, Meheus L, De Brabandere V, Fischer U, Lührmann R. Symmetrical dimethylation of arginine residues in spliceosomal Sm protein B/B′ and the Sm-like protein LSm4, and their interaction with the SMN protein. RNA. 2001;7(11):1531–42.
38. Brahms H, Raymackers J, Union A, De Keyser F, Meheus L, Luhrmann R. The C-terminal RG dipeptide repeats of the spliceosomal Sm proteins D1 and D3 contain symmetrical dimethylarginines, which form a major B-cell epitope for anti-Sm autoantibodies. J Biol Chem. 2000;275(22):17122–9.
39. Lorson CL, Strasswimmer J, Yao JM, Baleja JD, Hahnen E, Wirth B, Le T, Burghes AH, Androphy EJ. SMN oligomerization defect correlates with spinal muscular atrophy severity. Nat Genet. 1998;19(1):63–6.
40. Martin R, Gupta K, Ninan NS, Perry K, Van Duyne GD. The survival motor neuron protein forms soluble glycine zipper oligomers. Structure. 2012;20(11):1929–39.
41. Hanson MA, Cohen LB, Marra A, Iatsenko I, Wasserman SA, Lemaitre B. The Drosophila Baramicin polypeptide gene protects against fungal infection. PLoS Pathog. 2021;17(8):e1009846.
42. Hanson MA, Lemaitre B. Repeated truncation of a modular antimicrobial peptide gene for neural context. PLoS Genet. 2022;18(6):e1010259.
43. Li L, Ding Z, Pang TL, Zhang B, Li CH, Liang AM, Wang YR, Zhou Y, Fan YJ, Xu YZ. Defective minor spliceosomes induce SMA-associated phenotypes through sensitive intron-containing neural genes in Drosophila. Nat Commun. 2020;11(1):5608.
44. Bray NL, Pimentel H, Melsted P, Pachter L. Near-optimal probabilistic RNA-seq quantification. Nat Biotechnol. 2016;34(5):525–7.
45. Pimentel H, Bray NL, Puente S, Melsted P, Pachter L. Differential analysis of RNA-seq incorporating quantification uncertainty. Nat Methods. 2017;14(7):687–90.
46. Minakhina S, Steward R. Melanotic mutants in Drosophila: pathways and phenotypes. Genetics. 2006;174(1):253–63.
47. Boulet M, Miller M, Vandel L, Waltzer L. From drosophila blood cells to human leukemia. Adv Exp Med Biol. 2018;1076:195–214.
48. Gold KS, Brückner K: Macrophages and cellular immunity in Drosophila melanogaster. In: Seminars in Immunology. Elsevier. 2015: 357–368.
49. Williams MJ. Drosophila hemopoiesis and cellular immunity. J Immunol. 2007;178(8):4711–6.
50. Banerjee U, Girard JR, Goins LM, Spratford CM. Drosophila as a genetic model for hematopoiesis. Genetics. 2019;211(2):367–417.
51. Perkins LA, Holderbaum L, Tao R, Hu Y, Sopko R, McCall K, Yang-Zhou D, Flockhart I, Binari R, Shim HS, et al. The transgenic RNAi project at Harvard Medical School: resources and validation. Genetics. 2015;201(3):843–52.
52. Dimitriadi M, Sleigh JN, Walker A, Chang HC, Sen A, Kalloo G, Harris J, Barsby T, Walsh MB, Satterlee JS, et al. Conserved genes act as modifiers of invertebrate SMN loss of function defects. PLoS Genet. 2010;6(10):e1001172.
53. Brusich DJ, Spring AM, Frank CA. A single-cross, RNA interference-based genetic tool for examining the long-term maintenance of homeostatic plasticity. Front Cell Neurosci. 2015;9:107.
54. Asha H, Nagy I, Kovacs G, Stetson D, Ando I, Dearolf CR. Analysis of Ras-induced overproliferation in Drosophila hemocytes. Genetics. 2003;163(1):203–15.
55. Hoffmann JA, Reichhart JM. Drosophila innate immunity: an evolutionary perspective. Nat Immunol. 2002;3(2):121–6.
56. Ferrandon D, Imler JL, Hetru C, Hoffmann JA. The Drosophila systemic immune response: sensing and signalling during bacterial and fungal infections. Nat Rev Immunol. 2007;7(11):862–74.
57. Hanson MA, Lemaitre B. New insights on Drosophila antimicrobial peptide function in host defense and beyond. Curr Opin Immunol. 2020;62:22–30.
58. Lemaitre B, Hoffmann J. The host defense of Drosophila melanogaster. Annu Rev Immunol. 2007;25:697–743.
59. Lindsay SA, Wasserman SA. Conventional and non-conventional Drosophila toll signaling. Dev Comp Immunol. 2014;42(1):16–24.
60. Nicolas E, Reichhart JM, Hoffmann JA, Lemaitre B. In vivo regulation of the IkappaB homologue cactus during the immune response of Drosophila. J Biol Chem. 1998;273(17):10463–9.
61. Shpargel KB, Praveen K, Rajendra TK, Matera AG. Gemin3 is an essential gene required for larval motor function and pupation in Drosophila. Mol Biol Cell. 2009;20(1):90–101.
62. Matera AG, Raimer AC, Schmidt CA, Kelly JA, Droby GN, Baillat D, Ten Have S, Lamond AI, Wagner EJ, Gray KM. Composition of the Survival Motor Neuron (SMN) complex in drosophila melanogaster. G3 (Bethesda). 2019;9(2):491–503.
63. Gonsalvez GB, Rajendra TK, Tian L, Matera AG. The Sm-protein methyltransferase, dart5, is essential for germ-cell specification and maintenance. Curr Biol: CB. 2006;16(11):1077–89.
64. Guruharsha KG, Rual JF, Zhai B, Mintseris J, Vaidya P, Vaidya N, Beekman C, Wong C, Rhee DY, Cenaj O, et al. A protein complex network of Drosophila melanogaster. Cell. 2011;147(3):690–703.
65. Friesen WJ, Massenet S, Paushkin S, Wyce A, Dreyfuss G. SMN, the product of the spinal muscular atrophy gene, binds preferentially to dimethylarginine-containing protein targets. Mol Cell. 2001;7(5):1111–7.
66. Meister G, Eggert C, Buhler D, Brahms H, Kambach C, Fischer U. Methylation of Sm proteins by a complex containing PRMT5 and the putative U snRNP assembly factor pICln. Curr Biol: CB. 2001;11(24):1990–4.
67. Gonsalvez GB, Praveen K, Hicks AJ, Tian L, Matera AG. Sm protein methylation is dispensable for snRNP assembly in Drosophila melanogaster. RNA. 2008;14(5):878–87.
68. Shen B, Liu H, Skolnik EY, Manley JL. Physical and functional interactions between Drosophila TRAF2 and Pelle kinase contribute to Dorsal activation. Proc Natl Acad Sci USA. 2001;98(15):8596–601.
69. Cha GH, Cho KS, Lee JH, Kim M, Kim E, Park J, Lee SB, Chung J. Discrete functions of TRAF1 and TRAF2 in Drosophila melanogaster mediated by c-Jun N-terminal kinase and NF-kappaB-dependent signaling pathways. Mol Cell Biol. 2003;23(22):7982–91.
70. Ma X, Li W, Yu H, Yang Y, Li M, Xue L, Xu T. Bendless modulates JNK-mediated cell death and migration in Drosophila. Cell Death Differ. 2014;21(3):407–15.
71. Ding X, Li Z, Lin G, Li W, Xue L. Toll-7 promotes tumour growth and invasion in Drosophila. Cell Prolif. 2022;55(2): e13188.
72. Igaki T, Miura M. The Drosophila TNF ortholog Eiger: emerging physiological roles and evolution of the TNF system. Semin Immunol. 2014;26(3):267–74.
73. Sharma V, Mutsuddi M, Mukherjee A. Deltex cooperates with TRAF6 to promote apoptosis and cell migration through Eiger-independent JNK activation in Drosophila. Cell Biol Int. 2021;45(3):686–700.
74. Kauppila S, Maaty WS, Chen P, Tomar RS, Eby MT, Chapo J, Chew S, Rathore N, Zachariah S, Sinha SK, et al. Eiger and its receptor, Wengen, comprise a TNF-like system in Drosophila. Oncogene. 2003;22(31):4860–7.

75. Zhou R, Silverman N, Hong M, Liao DS, Chung Y, Chen ZJ, Maniatis T. The role of ubiquitination in Drosophila innate immunity. J Biol Chem. 2005;280(40):34048–55.
76. Chen L, Paquette N, Mamoor S, Rus F, Nandy A, Leszyk J, Shaffer SA, Silverman N. Innate immune signaling in Drosophila is regulated by transforming growth factor beta (TGFbeta)-activated kinase (Tak1)-triggered ubiquitin editing. J Biol Chem. 2017;292(21):8738–49.
77. Kim EK, Choi EJ. SMN1 functions as a novel inhibitor for TRAF6-mediated NF-kappaB signaling. Biochim Biophys Acta Mol Cell Res. 2017;1864(5):760–70.
78. Vukojicic A, Delestree N, Fletcher EV, Pagiazitis JG, Sankaranarayanan S, Yednock TA, Barres BA, Mentis GZ. The classical complement pathway mediates microglia-dependent remodeling of spinal motor circuits during development and in SMA. Cell reports. 2019;29(10):3087–100 e3087.
79. Zhang Z, Pinto AM, Wan L, Wang W, Berg MG, Oliva I, Singh LN, Dengler C, Wei Z, Dreyfuss G. Dysregulation of synaptogenesis genes antecedes motor neuron pathology in spinal muscular atrophy. Proc Natl Acad Sci USA. 2013;110(48):19348–53.
80. Scharf JM, Endrizzi MG, Wetter A, Huang S, Thompson TG, Zerres K, Dietrich WF, Wirth B, Kunkel LM. Identification of a candidate modifying gene for spinal muscular atrophy by comparative genomics. Nat Genet. 1998;20(1):83–6.
81. Ahmad S, Wang Y, Shaik GM, Burghes AH, Gangwani L. The zinc finger protein ZPR1 is a potential modifier of spinal muscular atrophy. Hum Mol Genet. 2012;21(12):2745–58.
82. Zhuri D, Gurkan H, Eker D, Karal Y, Yalcintepe S, Atli E, Demir S, Atli EI. Investigation on the effects of modifying genes on the spinal muscular atrophy phenotype. Glob Med Genet. 2022;9(3):226–36.
83. Hosseinibarkooie S, Peters M, Torres-Benito L, Rastetter RH, Hupperich K, Hoffmann A, Mendoza-Ferreira N, Kaczmarek A, Janzen E, Milbradt J, et al. The power of human protective modifiers: PLS3 and CORO1C unravel impaired endocytosis in spinal muscular atrophy and rescue SMA phenotype. Am J Hum Genet. 2016;99(3):647–65.
84. Wirth B, Karakaya M, Kye MJ, Mendoza-Ferreira N. Twenty-five years of spinal muscular atrophy research: from phenotype to genotype to therapy, and what comes next. Annu Rev Genomics Hum Genet. 2020;21:231–61.
85. Ghosh S. Genetic analysis of Serf gene function in Drosophila melanogaster and its contribution to a fly model of Spinal Muscular Atrophy. Lexington: University of Kentucky; 2017.
86. Liu Q, Kausar S, Tang Y, Huang W, Tang B, Abbas MN, Dai L. The emerging role of STING in insect innate immune responses and pathogen evasion strategies. Front Immunol. 2022;13:874605.
87. Zhao DY, Gish G, Braunschweig U, Li Y, Ni Z, Schmitges FW, Zhong G, Liu K, Li W, Moffat J, et al. SMN and symmetric arginine dimethylation of RNA polymerase II C-terminal domain control termination. Nature. 2016;529(7584):48–53.
88. Kannan A, Jiang X, He L, Ahmad S, Gangwani L. ZPR1 prevents R-loop accumulation, upregulates SMN2 expression and rescues spinal muscular atrophy. Brain. 2020;143(1):69–93.
89. Cuartas J, Gangwani L. R-loop mediated DNA damage and impaired DNA repair in spinal muscular atrophy. Front Cell Neurosci. 2022;16:826608.
90. Gangwani L, Mikrut M, Theroux S, Sharma M, Davis RJ. Spinal muscular atrophy disrupts the interaction of ZPR1 with the SMN protein. Nat Cell Biol. 2001;3(4):376–83.
91. Narayanan U, Ospina JK, Frey MR, Hebert MD, Matera AG. SMN, the spinal muscular atrophy protein, forms a pre-import snRNP complex with snurportin1 and importin beta. Hum Mol Genet. 2002;11(15):1785–95.
92. Crossley MP, Song C, Bocek MJ, Choi JH, Kousouros JN, Sathirachinda A, Lin C, Brickner JR, Bai G, Lans H, et al. R-loop-derived cytoplasmic RNA-DNA hybrids activate an immune response. Nature. 2023;613(7942):187–94.
93. Martin M, Hiroyasu A, Guzman RM, Roberts SA, Goodman AG. Analysis of Drosophila STING reveals an evolutionarily conserved antimicrobial function. Cell reports. 2018;23(12):3537–50. e3536.
94. Hua X, Li B, Song L, Hu C, Li X, Wang D, Xiong Y, Zhao P, He H, Xia Q, et al. Stimulator of interferon genes (STING) provides insect antiviral immunity by promoting Dredd caspase-mediated NF-kappaB activation. J Biol Chem. 2018;293(30):11878–90.
95. Slavik KM, Morehouse BR, Ragucci AE, Zhou W, Ai X, Chen Y, Li L, Wei Z, Bahre H, Konig M, et al. cGAS-like receptors sense RNA and control 3'2'-cGAMP signalling in Drosophila. Nature. 2021;597(7874):109–13.
96. Liu Y, Gordesky-Gold B, Leney-Greene M, Weinbren NL, Tudor M, Cherry S. Inflammation-induced, STING-dependent autophagy restricts Zika virus infection in the Drosophila brain. Cell Host Microbe. 2018;24(1):57–68. e53.
97. Liu Y, Cherry S. Zika virus infection activates sting-dependent antiviral autophagy in the Drosophila brain. Autophagy. 2019;15(1):174–5.
98. Cai H, Holleufer A, Simonsen B, Schneider J, Lemoine A, Gad HH, Huang J, Huang J, Chen D, Peng T et al: 2'3'-cGAMP triggers a STING- and NF-kappaB-dependent broad antiviral response in Drosophila. Sci Signal. 2020;13(660):eabc4537.
99. Tan L, Schedl P, Song HJ, Garza D, Konsolaki M. The Toll–>NFkappaB signaling pathway mediates the neuropathological effects of the human Alzheimer's Abeta42 polypeptide in Drosophila. PLoS ONE. 2008;3(12):e3966.
100. Xie X, Ma G, Li X, Zhao J, Zhao Z, Zeng J. Activation of innate immune cGAS-STING pathway contributes to Alzheimer's pathogenesis in 5xFAD mice. Nat Aging. 2023;3(2):202–12.
101. Swarup V, Phaneuf D, Dupre N, Petri S, Strong M, Kriz J, Julien JP. Deregulation of TDP-43 in amyotrophic lateral sclerosis triggers nuclear factor kappaB-mediated pathogenic pathways. J Exp Med. 2011;208(12):2429–47.
102. Egawa N, Kitaoka S, Tsukita K, Naitoh M, Takahashi K, Yamamoto T, Adachi F, Kondo T, Okita K, Asaka I, et al. Drug screening for ALS using patient-specific induced pluripotent stem cells. Sci Transl Med. 2012;4(145):145ra104.
103. Zhao W, Beers DR, Bell S, Wang J, Wen S, Baloh RH, Appel SH. TDP-43 activates microglia through NF-kappaB and NLRP3 inflammasome. Exp Neurol. 2015;273:24–35.
104. Yu CH, Davidson S, Harapas CR, Hilton JB, Mlodzianoski MJ, Laohamonthonkul P, Louis C, Low RRJ, Moecking J, De Nardo D, et al. TDP-43 triggers mitochondrial DNA release via mPTP to activate cGAS/STING in ALS. Cell. 2020;183(3):636–49. e618.
105. Lee JD, Woodruff TM. TDP-43 puts the STING in ALS. Trends Neurosci. 2021;44(2):81–2.
106. Petersen AJ, Rimkus SA, Wassarman DA. ATM kinase inhibition in glial cells activates the innate immune response and causes neurodegeneration in Drosophila. Proc Natl Acad Sci USA. 2012;109(11):E656-664.
107. Petersen AJ, Wassarman DA. Drosophila innate immune response pathways moonlight in neurodegeneration. Fly (Austin). 2012;6(3):169–72.
108. Han MH, Kwon MJ, Ko BS, Hyeon DY, Lee D, Kim HJ, Hwang D, Lee SB: NF-kappaB disinhibition contributes to dendrite defects in fly models of neurodegenerative diseases. J Cell Biol 2020;219(12):e202004107.
109. Chinchore Y, Gerber GF, Dolph PJ. Alternative pathway of cell death in Drosophila mediated by NF-kappaB transcription factor Relish. Proc Natl Acad Sci USA. 2012;109(10):E605-612.
110. Cai H, Meignin C, Imler JL. cGAS-like receptor-mediated immunity: the insect perspective. Curr Opin Immunol. 2022;74:183–9.
111. Wang L, Tracy L, Su W, Yang F, Feng Y, Silverman N, Zhang ZZZ. Retrotransposon activation during Drosophila metamorphosis conditions adult antiviral responses. Nat Genet. 2022;54(12):1933–45.
112. Valanne S, Wang JH, Ramet M. The Drosophila Toll signaling pathway. J Immunol. 2011;186(2):649–56.
113. Kietz C, Meinander A. Drosophila caspases as guardians of host-microbe interactions. Cell Death Differ. 2023;30(2):227–36.
114. Leulier F, Lhocine N, Lemaitre B, Meier P. The Drosophila inhibitor of apoptosis protein DIAP2 functions in innate immunity and is essential to resist gram-negative bacterial infection. Mol Cell Biol. 2006;26(21):7821–31.
115. Paquette N, Broemer M, Aggarwal K, Chen L, Husson M, Erturk-Hasdemir D, Reichhart JM, Meier P, Silverman N. Caspase-mediated cleavage, IAP binding, and ubiquitination: linking three mechanisms crucial for Drosophila NF-kappaB signaling. Mol Cell. 2010;37(2):172–82.
116. Strickson S, Emmerich CH, Goh ETH, Zhang J, Kelsall IR, Macartney T, Hastie CJ, Knebel A, Peggie M, Marchesi F, et al. Roles of the TRAF6 and Pellino E3 ligases in MyD88 and RANKL signaling. Proc Natl Acad Sci USA. 2017;114(17):E3481–9.

117. Cao Y, Chtarbanova S, Petersen AJ, Ganetzky B. Dnr1 mutations cause neurodegeneration in Drosophila by activating the innate immune response in the brain. Proc Natl Acad Sci USA. 2013;110(19):E1752-1760.
118. Mertins P, Tang LC, Krug K, Clark DJ, Gritsenko MA, Chen L, Clauser KR, Clauss TR, Shah P, Gillette MA. Reproducible workflow for multiplexed deep-scale proteome and phosphoproteome analysis of tumor tissues by liquid chromatography–mass spectrometry. Nat Protoc. 2018;13(7):1632–61.
119. McAlister GC, Nusinow DP, Jedrychowski MP, Wühr M, Huttlin EL, Erickson BK, Rad R, Haas W, Gygi SP. MultiNotch MS3 enables accurate, sensitive, and multiplexed detection of differential expression across cancer cell line proteomes. Anal Chem. 2014;86(14):7150–8.
120. Chen EY, Tan CM, Kou Y, Duan Q, Wang Z, Meirelles GV, Clark NR, Ma'ayan A. Enrichr: interactive and collaborative HTML5 gene list enrichment analysis tool. BMC Bioinformatics. 2013;14(1):1–14.
121. Kuleshov MV, Jones MR, Rouillard AD, Fernandez NF, Duan Q, Wang Z, Koplev S, Jenkins SL, Jagodnik KM, Lachmann A. Enrichr: a comprehensive gene set enrichment analysis web server 2016 update. Nucleic Acids Res. 2016;44(W1):W90–7.
122. Adams MD, Celniker SE, Holt RA, Evans CA, Gocayne JD, Amanatides PG, Scherer SE, Li PW, Hoskins RA, Galle RF, et al. The genome sequence of Drosophila melanogaster. Science. 2000;287(5461):2185–95.
123. Kim D, Paggi JM, Park C, Bennett C, Salzberg SL. Graph-based genome alignment and genotyping with HISAT2 and HISAT-genotype. Nat Biotechnol. 2019;37(8):907–15.
124. Love MI, Huber W, Anders S. Moderated estimation of fold change and dispersion for RNA-seq data with DESeq2. Genome Biol. 2014;15(12):1–21.
125. Pertea M, Pertea GM, Antonescu CM, Chang T-C, Mendell JT, Salzberg SL. StringTie enables improved reconstruction of a transcriptome from RNA-seq reads. Nat Biotechnol. 2015;33(3):290–5.
126. Gupta K, Martin R, Sharp R, Sarachan KL, Ninan NS, Van Duyne GD. Oligomeric properties of survival motor neuron.Gemin2 complexes. J Biol Chem. 2015;290(33):20185–99.
127. Perez-Riverol Y, Bai J, Bandla C, García-Seisdedos D, Hewapathirana S, Kamatchinathan S, Kundu DJ, Prakash A, Frericks-Zipper A, Eisenacher M. The PRIDE database resources in 2022: a hub for mass spectrometry-based proteomics evidences. Nucleic Acids Res. 2022;50(D1):D543–52.

Publisher's Note